Title
CLSTN3β enforces adipocyte multilocularity to facilitate lipid utilization.

Journal
Nature, 613(7942)

ISSN
0028-0836

Authors
Qian, Kevin
Tol, Marcus J
Wu, Jin
et al.

Publication Date
2023

DOI
10.1038/s41586-022-05507-1

Article

CLSTN3β enforces adipocyte multilocularity to facilitate lipid utilization

https://doi.org/10.1038/s41586-022-05507-1

Received: 11 November 2021

Accepted: 1 November 2022

Published online: 7 December 2022

Check for updates

Kevin Qian[1,2,3], Marcus J. Tol[1,2,3], Jin Wu[4], Lauren F. Uchiyama[1,2,3], Xu Xiao[1,2,3], Liujuan Cui[1,2,3], Alexander H. Bedard[1,2,3], Thomas A. Weston[5,6], Pradeep S. Rajendran[7,8], Laurent Vergnes[6], Yuta Shimanaka[1,2,3], Yesheng Yin[4], Yasaman Jami-Alahmadi[2], Whitaker Cohn[9], Bryce T. Bajar[2], Chia-Ho Lin[10], Benita Jin[11], Laura A. DeNardo[11], Douglas L. Black[10], Julian P. Whitelegge[9], James A. Wohlschlegel[2], Karen Reue[6], Kalyanam Shivkumar[7], Feng-Jung Chen[4], Stephen G. Young[5,6], Peng Li[4,12] & Peter Tontonoz[1,2,3]✉

Multilocular adipocytes are a hallmark of thermogenic adipose tissue[1,2], but the factors that enforce this cellular phenotype are largely unknown. Here, we show that an adipocyte-selective product of the *Clstn3* locus (CLSTN3β) present in only placental mammals facilitates the efficient use of stored triglyceride by limiting lipid droplet (LD) expansion. CLSTN3β is an integral endoplasmic reticulum (ER) membrane protein that localizes to ER–LD contact sites through a conserved hairpin-like domain. Mice lacking CLSTN3β have abnormal LD morphology and altered substrate use in brown adipose tissue, and are more susceptible to cold-induced hypothermia despite having no defect in adrenergic signalling. Conversely, forced expression of CLSTN3β is sufficient to enforce a multilocular LD phenotype in cultured cells and adipose tissue. CLSTN3β associates with cell death-inducing DFFA-like effector proteins and impairs their ability to transfer lipid between LDs, thereby restricting LD fusion and expansion. Functionally, increased LD surface area in CLSTN3β-expressing adipocytes promotes engagement of the lipolytic machinery and facilitates fatty acid oxidation. In human fat, *CLSTN3B* is a selective marker of multilocular adipocytes. These findings define a molecular mechanism that regulates LD form and function to facilitate lipid utilization in thermogenic adipocytes.

Decades before its thermogenic function was described, brown adipose tissue (BAT) was recognized to have a distinct histological appearance, characterized by "densely packed polygonal cells … in which there are usually a large number of fat globules of various sizes" (refs. [3–5]). Today, the presence of multilocular adipocytes is considered a hallmark of thermogenic fat. This feature distinguishes brown/beige adipocytes morphologically from unilocular, energy-storing white adipocytes[1,2]. The organization of intracellular lipid stores into many small LDs is postulated to improve the efficiency of triglyceride use by increasing the LD surface area-to-volume ratio[6,7]. However, this hypothesis has not been formally tested, largely because the mechanism by which thermogenic adipocytes enforce a multilocular phenotype is still unknown.

In the main lipid-storing cells, LD expansion is governed by cell death-inducing DFFA-like effector (CIDE) proteins—LD-associated proteins that mediate LD–LD contact and net lipid transfer from small to large LDs over time[8–13]. White adipocytes express high amounts of CIDEC; brown/beige adipocytes have abundant CIDEA/C and hepatocytes express CIDEB and induce CIDEA/C in fatty liver[14–18]. All three CIDEs perform the same basic function of facilitating LD fusion, and CIDE deficiency results in accumulation of small LDs in various cell types in both mice and humans[11,12,14,19–25]. Given the divergent outcomes of high CIDE expression in white and brown/beige adipocytes in terms of LD morphology, it is likely that thermogenic fat cells contain as-yet-undefined factors that modify CIDE activity in a cell type-specific manner[6].

Here, we identify calsyntenin-3β (CLSTN3β) as a critical determinant of the multilocular LD phenotype and efficient lipid use characteristic of thermogenic adipocytes. CLSTN3β localizes to ER–LD contact sites, where it constrains LD expansion by blocking CIDE-mediated LD fusion. Loss of CLSTN3β expression leads to abnormal BAT LD morphology and impaired thermogenesis, whereas forced expression of CLSTN3β promotes multilocularity and fatty acid oxidation. These findings provide a mechanistic basis for understanding how certain adipocyte populations enforce a multilocular phenotype, thereby maximizing LD surface area, lipid use and thermogenesis.

[1]Department of Pathology and Laboratory Medicine, University of California, Los Angeles, Los Angeles, CA, USA. [2]Department of Biological Chemistry, University of California, Los Angeles, Los Angeles, CA, USA. [3]Molecular Biology Institute, University of California, Los Angeles, Los Angeles, CA, USA. [4]Institute of Metabolism and Integrative Biology, Fudan University, Shanghai, China. [5]Department of Medicine, Division of Cardiology, University of California, Los Angeles, Los Angeles, CA, USA. [6]Department of Human Genetics, University of California, Los Angeles, Los Angeles, CA, USA. [7]Cardiac Arrhythmia Center and Neurocardiology Research Program of Excellence, University of California, Los Angeles, Los Angeles, CA, USA. [8]Department of Medicine, Massachusetts General Hospital, Boston, MA, USA. [9]Pasarow Mass Spectrometry Laboratory, Semel Institute for Neuroscience and Human Behavior, University of California, Los Angeles, Los Angeles, CA, USA. [10]Department of Microbiology, Immunology, and Molecular Genetics, University of California, Los Angeles, Los Angeles, CA, USA. [11]Department of Physiology, University of California, Los Angeles, Los Angeles, CA, USA. [12]School of Life Sciences, Tsinghua University, Beijing, China. ✉e-mail: ptontonoz@mednet.ucla.edu

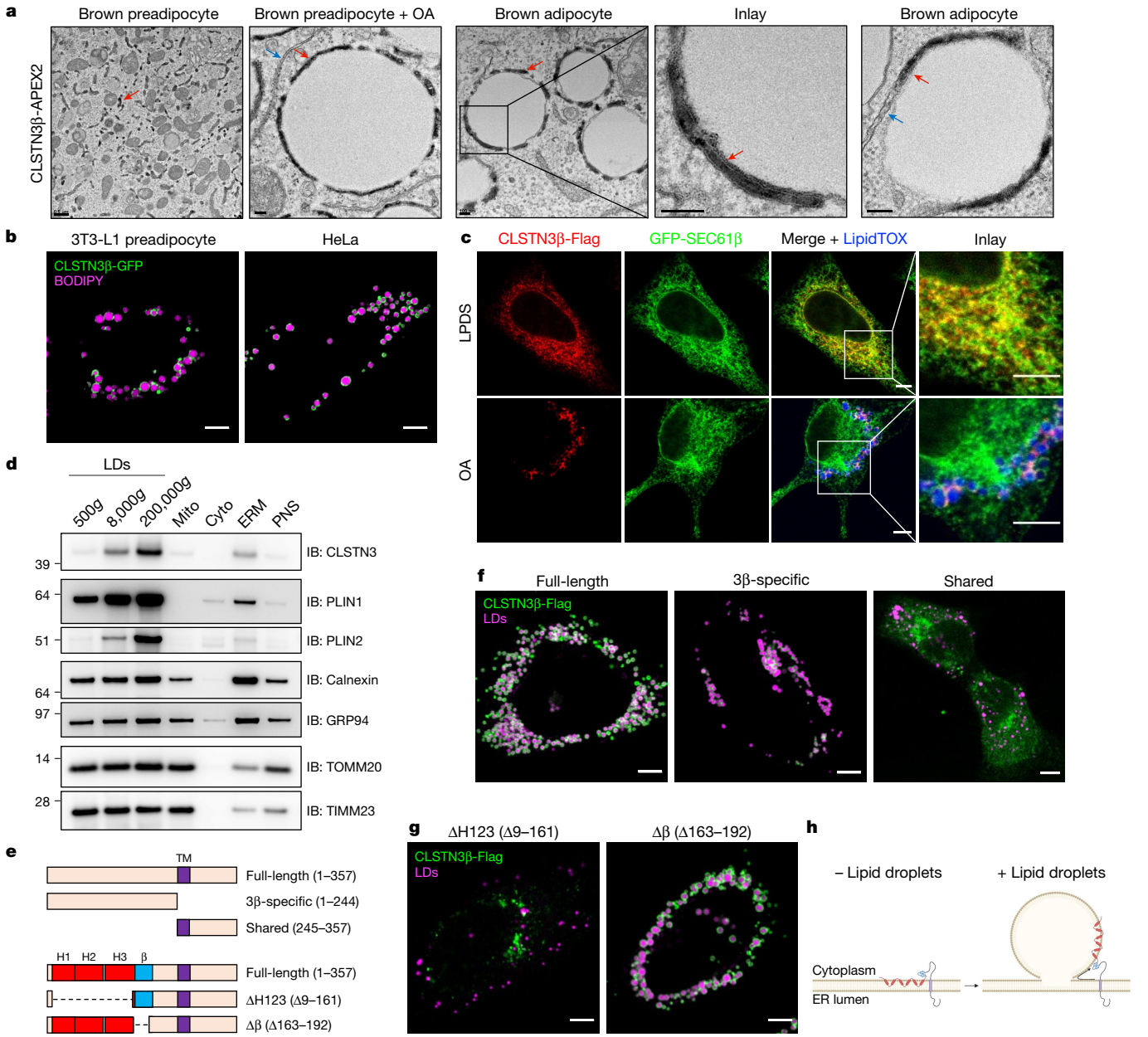

Fig. 1 | CLSTN3β is an ER-resident protein that localizes to ER–LD contact sites. a, Electron microscopy of immortalized brown preadipocytes stably expressing a CLSTN3β–APEX2 C-terminal fusion. Red and blue arrows point to ER tubules that are positive and negative for APEX2 product, respectively. From left to right are the untreated, treated with OA (1 mM, 2 h) and differentiated for 4 days. Scale bar, 0.5 µm (left panel); 100 nm (right four panels). **b**, Confocal microscopy of OA-treated 3T3-L1 preadipocytes and HeLa cells transfected with CLSTN3β-GFP and stained with BODIPY 665. Scale bar, 5 µm. **c**, Confocal microscopy of HeLa cells transfected with CLSTN3β-Flag and GFP-SEC61β and stained with LipidTOX 647. Cells were treated with lipoprotein-deficient serum (LPDS, 1%, overnight) (top) or OA (1 mM, overnight) (bottom). Scale bar, 5 µm. **d**, Western blot analysis of subcellular fractions from immortalized brown preadipocytes differentiated for 8 days. Similar amounts of protein from each fraction were loaded onto the gels (as estimated by silver stain). mito, mitochondria; cyto, cytoplasm; ERM, ER-enriched membranes; PNS, postnuclear supernatant. **e**, Schematic of full-length CLSTN3β and CLSTN3β mutants. TM, transmembrane domain; H1/H2/H3, hydrophobic hairpin 1/2/3; β, β-strand domain. **f**, Confocal microscopy of OA-treated (1 mM, overnight) HeLa cells transfected with full-length, 3β-specific or shared CLSTN3β-Flag constructs and stained with BODIPY 488 or LipidTOX 647. Scale bar, 5 µm. **g**, Confocal microscopy of OA-treated (1 mM, overnight) HeLa cells transfected with ΔH123 or Δβ CLSTN3β-Flag constructs and stained with BODIPY 488 or LipidTOX 647. Scale bar, 5 µm. **h**, Proposed CLSTN3β domain structure and mechanism of localization to ER–LD contact sites. Schematic created using BioRender (https://biorender.com).

Clstn3b is regulated by cold and PPARγ

CLSTN3β is an adipocyte-selective product of the *Clstn3* locus[26]. We independently identified *Clstn3* as a gene highly upregulated during brown adipocyte differentiation (Extended Data Fig. 1a). Visualization of RNA-sequencing reads mapping to the *Clstn3* locus in brown adipocytes revealed an alternative transcript (hereafter *Clstn3b*) containing a previously unannotated exon linked to exons 17 and 18 of the known *Clstn3* isoform. Assay for transposase-accessible chromatin, cap analysis of gene expression (CAGE) and H3K4me3 chromatin immunoprecipitation (ChIP) sequencing confirmed that *Clstn3b* arises from an alternative promoter within intron 16 (Extended Data Fig. 1a).

We annotated *Clstn3b* transcripts in BAT (Extended Data Fig. 1b) using complementary approaches. Comparative genome-wide splicing analysis[27] in cerebral cortex and BAT identified 1,284 intron clusters in which splice site use differed between the two tissues (Supplementary

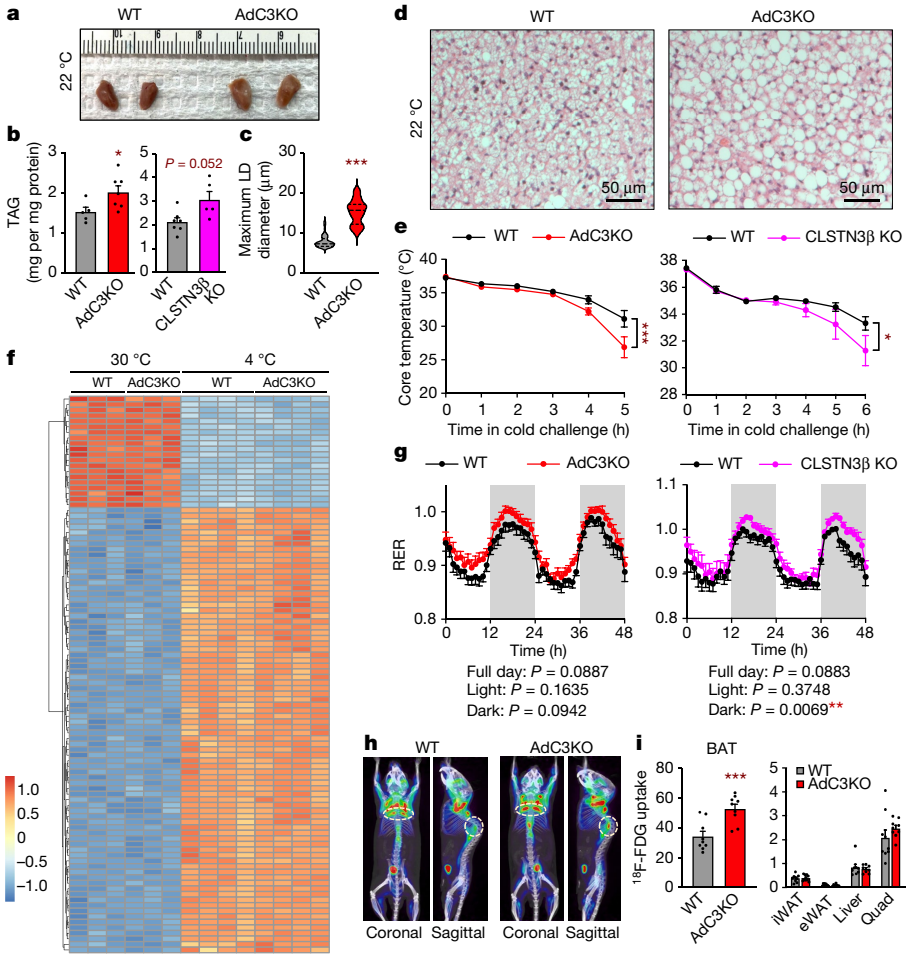

Fig. 2 | Loss of CLSTN3β expression perturbs LD morphology and lipid utilization in BAT. a, Gross appearance of BAT from 12-week-old male WT and AdC3KO mice housed at 22 °C. **b**, BAT triglyceride (TAG) content in 11–12-week-old male WT and AdC3KO mice ($n = 5, 7$) (left) and 17–18-week-old male WT and CLSTN3β KO mice ($n = 7, 5$) (right) housed at 22 °C. **c**,**d**, Diameters of largest LDs ($n = 60, 60$) (**c**) in H&E sections (**d**) of BAT from 11–12-week-old male WT and AdC3KO mice housed at 22 °C. Scale bar, 50 μm. **e**, Core body temperatures of 13–14-week-old male WT and AdC3KO mice ($n = 12, 12$) (left) and 12–13-week-old male WT and CLSTN3β KO mice ($n = 10, 11$) (right) during acute cold challenge. **f**, Heatmap of 100 most significantly changed genes in BAT during acute cold challenge. RNA sequencing was performed on BAT from 10-week-old male WT and AdC3KO mice ($n = 3, 3, 4, 4$). **g**, Respiratory exchange ratios (RER) of 10–12-week-old male WT and AdC3KO mice ($n = 18, 22$) (left) and 11–12-week-old male WT and CLSTN3β KO mice ($n = 13, 11$) (right) housed at 22 °C. **h**, Coronal and sagittal views of representative WT and AdC3KO mice undergoing ^{18}F-fluorodeoxyglucose (^{18}F-FDG) PET–CT after 4 h of cold exposure. BAT depots are circled. **i**, ^{18}F-FDG uptake (10^6 pCi per g of tissue) in BAT (left) and iWAT, epididymal WAT (eWAT), liver and quad (right) from 12–16-week-old male WT and AdC3KO mice housed at 4 °C for 4 h ($n = 9, 9$). Bar and line plots show mean ± s.e.m. Each point represents a biological replicate. Violin plots show median (dashed) and quartiles (dotted). Two-sided $^*P < 0.05$, $^{**}P < 0.01$, $^{***}P < 0.001$ by Welch's *t*-test (**b**,**c**,**i**), two-way repeated measures analysis of variance (ANOVA) with Sidak's multiple comparisons test (**e**) or ANOVA (**g**).

Data 1). Intron 16 of *Clstn3* ranked eighth overall in differential splicing (Extended Data Fig. 1c). In cortex, the annotated intron 16 was used by 100% of *Clstn3* transcripts, whereas in BAT, three different splice sites corresponding to three distinct *Clstn3b* transcript variants were used at varying frequencies (Extended Data Fig. 1d). These transcript variants were verified by 5′ RNA ligase-mediated-rapid amplification of complementary DNA (cDNA) ends (5′ RLM-RACE) and PCR with reverse transcription (RT–PCR) (Extended Data Fig. 1e,f).

Western blot analysis of brown adipocytes using an antibody targeting the C terminus of CLSTN3 revealed one specific band with an apparent molecular weight of roughly 25 kDa in whole cell lysates, and an extra band at roughly 40 kDa after isolation of cellular membranes (Extended Data Fig. 2a). Both species were encoded by a single *Clstn3b* transcript (variant 2, hereafter *Clstn3b*) (Extended Data Fig. 2b). These species were translated independently, with the roughly 40 kDa protein (hereafter CLSTN3β) and the roughly 25 kDa protein encoded by the longest and shortest open reading frames (ORFs), respectively (Extended Data Fig. 2c,d). A peptide from the previously unannotated region of CLSTN3β was identified by tandem mass spectrometry (MS/MS) analysis of the endogenous protein immunoprecipitated from brown adipocytes (Extended Data Fig. 2e,f).

Clstn3 expression was restricted to the brain, whereas *Clstn3b* was enriched in BAT, with lower levels of expression in liver and white adipose tissue (WAT) (Extended Data Fig. 2g). *Clstn3b* was upregulated in BAT and WAT as ambient temperature was decreased, an effect that was mimicked by β_3-adrenergic receptor agonism (Extended Data Fig. 2h,i). *Clstn3b* was also induced with adipocyte differentiation, short-term high-fat diet (HFD) and PPARγ agonism (Extended Data Fig. 2j–l). ChIP confirmed that PPARγ binds to the *Clstn3b* promoter, consistent with published ChIP-sequencing data (Extended Data Fig. 2m,n)[28].

CLSTN3β localizes to ER–LD contact sites

Electron microscopy of brown preadipocytes stably expressing a CLSTN3β-APEX2 (ref. [29]) C-terminal fusion revealed that CLSTN3β

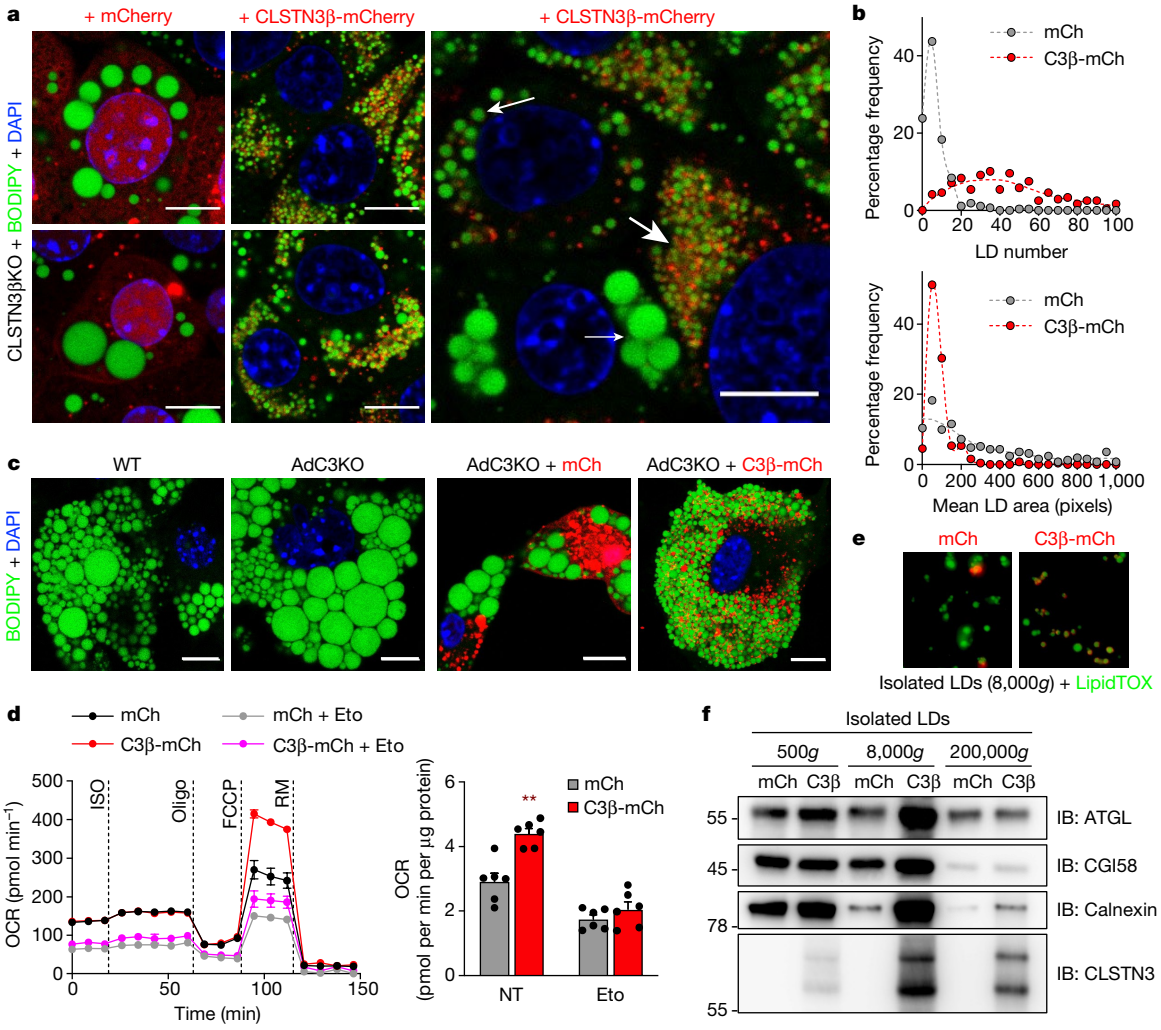

Fig. 3 | Forced expression of CLSTN3β promotes multilocularity and lipid utilization in adipocytes. a, Left, confocal microscopy of immortalized CLSTN3β KO brown adipocytes stably expressing mCherry (left) or CLSTN3β-mCherry (right) (day 5 of differentiation). Cells were stained with BODIPY 488 and DAPI, and mCherry signal was amplified with anti-mCherry Alexa Fluor 594. Right, cells with high CLSTN3β expression had the smallest LDs (large arrow), those with medium CLSTN3β expression had larger LDs (medium arrow) and those with low CLSTN3β expression had the largest LDs (small arrow). Scale bar, 10 μm. **b**, Frequency distribution of LD number (top) and mean LD size per cell in **a** (bottom). 272 and 244 cells were analysed for mCherry (mCh) and CLSTN3β-mCherry (C3β-mCh), respectively. **c**, Confocal microscopy of WT and AdC3KO primary brown adipocytes (day 6 of differentiation) (left) and AdC3KO primary brown adipocytes transduced with mCh or C3β-mCh lentivirus (day 4 of differentiation) (right). Cells were stained with BODIPY 488 and DAPI. Scale bar, 10 μm. **d**, Left, Seahorse respirometry analysis of oxygen consumption rate (OCR) in immortalized CLSTN3β KO brown adipocytes stably expressing mCh or C3β-mCh (day 6 of differentiation) and treated with isoproterenol (ISO, 10 μM), oligomycin (oligo, 4 μM), FCCP (2 μM) and rotenone/myxothiazol (RM, 7.5 μM). Cells were pretreated with etomoxir (Eto, 10 μM) for 30–45 min where indicated. Right, FCCP-induced OCR normalized to protein content ($n = 6$). **e**,**f**, Fluorescence microscopy (**e**) and western blot analysis (**f**) of large (500*g*), medium (8,000*g*) and/or small (200,000*g*) LDs isolated from immortalized CLSTN3β KO brown adipocytes stably expressing mCh or C3β-mCh (day 8 of differentiation). Equal amounts of TAG from each condition were loaded onto the gels. Bar/line plots show mean ± s.e.m. Each point represents a biological replicate. Two-sided $^{**}P < 0.01$ by multiple *t*-tests with Holm–Sidak correction (**d**).

is an ER-resident protein oriented with its C terminus facing the ER lumen (Fig. 1a). However, once preadipocytes were stimulated to form LDs (by oleic acid (OA) treatment or differentiation), CLSTN3β localized exclusively to ER–LD contact sites and was depleted from adjacent ER tubules not associated with LDs (Fig. 1a and Extended Data Fig. 3a). CLSTN3β readily localized to LDs in a variety of cell types while maintaining colocalization with the ER (Fig. 1b,c). In OA-treated cells, CLSTN3β was resistant to biochemical extraction from membranes and its ER-luminal C terminus was protected from trypsin digestion (Extended Data Fig. 3b,c), confirming that CLSTN3β remains an integral ER membrane protein after it redistributes to LDs. Endogenous CLSTN3β also localizes to LDs, as it was highly enriched in LDs isolated from brown adipocytes (Fig. 1d).

To identify the domain of CLSTN3β that facilitates its association with LDs, we assessed the localization of a series of truncation mutants (Fig. 1e). We found that the N-terminal CLSTN3β-specific region was necessary and sufficient for localization to LDs (Fig. 1f), indicating that LD targeting is a unique feature of the β isoform of CLSTN3. On the basis of its lack of homology to other proteins, the CLSTN3β-specific region did not seem to contain domains of known function. TMHMM[30] predicted three more transmembrane domain helices; however, true transmembrane helices cannot localize to LDs, and none of these helices appeared to have amphipathic character that would enable LD binding (Extended Data Fig. 3d,e). Other secondary structure predictors[31–33] raised the possibility that the three predicted transmembrane helices were actually part of a group of three hydrophobic hairpins.

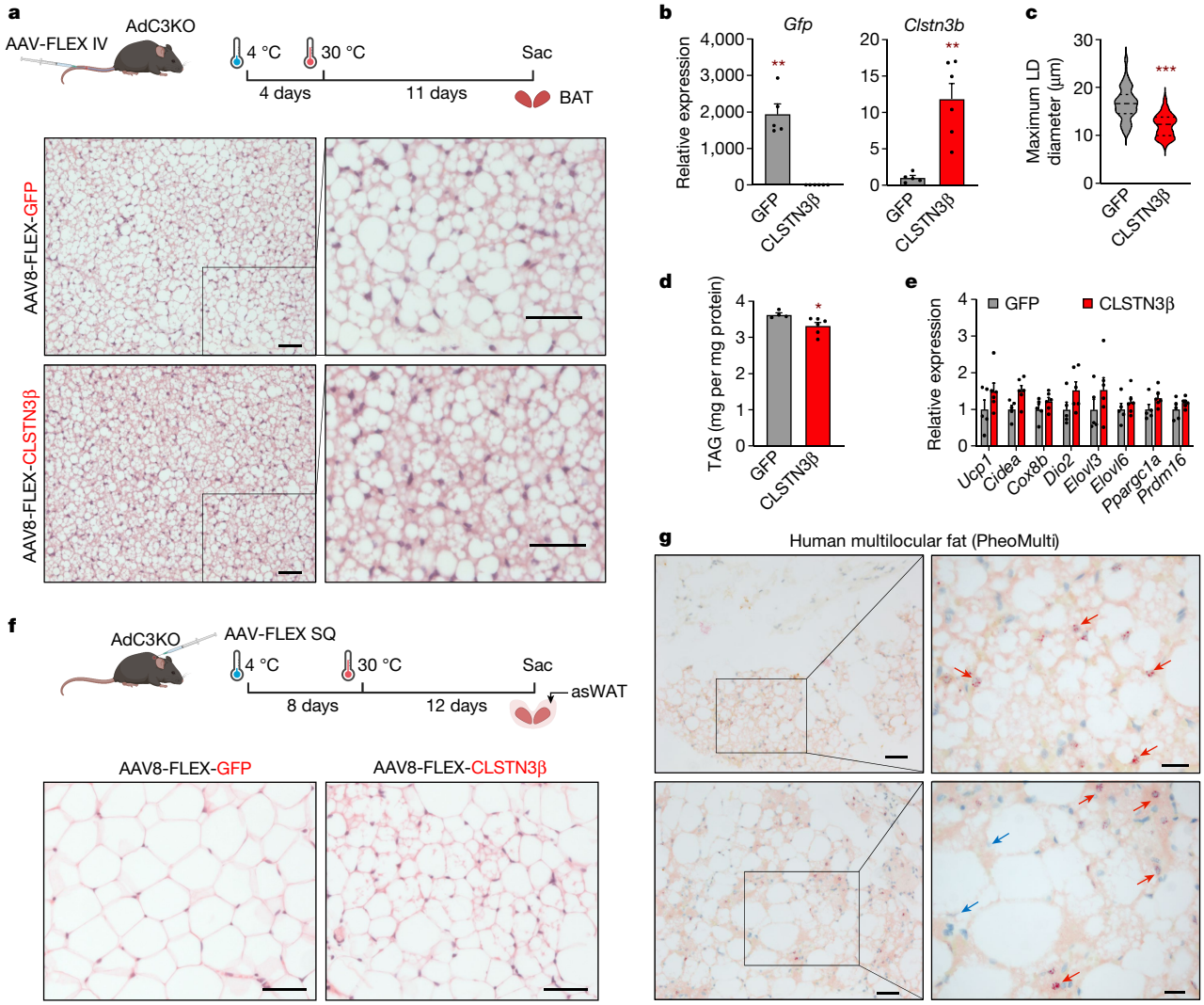

Fig. 4 | CLSTN3β expression is associated with multilocular adipose tissue in mice and humans. a–**e**, 10–14-week-old female AdC3KO mice were administered AAV8-FLEX-GFP or AAV8-FLEX-CLSTN3β-Flag ($n = 5, 6$) through the tail vein to express GFP or CLSTN3β-Flag specifically in adipocytes. Mice were housed at 4 °C for 4 days to minimize initial LD size, then housed at 30 °C for 11 days to promote LD expansion. **a**, Top, schematic of experiment. Bottom, H&E sections of BAT. Scale bar, 50 μm. **b**, Expression of AAV-encoded genes in BAT. **c**, Diameters of largest LDs in BAT ($n = 100, 120$). **d**, BAT TAG content. **e**, BAT thermogenic gene expression. **f**, 13–15-week-old male AdC3KO mice were administered AAV8-FLEX-GFP or AAV8-FLEX-CLSTN3β-Flag subcutaneously to express GFP or CLSTN3β-Flag specifically in adipocytes. Mice were housed at 4 °C for 8 days to induce beiging, then housed at 30 °C for 12 days to promote LD expansion. Top, schematic of experiment. Bottom, H&E sections of anterior subcutaneous WAT (asWAT). Scale bar, 50 μm. **g**, RNAscope analysis of *CLSTN3B* expression in multilocular periadrenal adipose tissue from patients with pheochromocytoma. Red arrows point to nuclei with positive staining in multilocular adipocytes. Blue arrows point to nuclei with negative staining in unilocular adipocytes. Scale bars, left 50 μm and right 20 μm. Bar plots show mean ± s.e.m. Each point represents a biological replicate. Violin plots show median (dashed) and quartiles (dotted). Two-sided $^{*}P < 0.05$, $^{**}P < 0.01$, $^{***}P < 0.001$ by Welch's *t*-test (**b**–**d**). Schematics in **a** and **f** created using BioRender (https://biorender.com).

RoseTTAFold[34] protein structure prediction supported this hypothesis (Extended Data Fig. 3f). The CLSTN3β-specific region was also predicted to contain positively charged amphipathic β-strands (Extended Data Fig. 3e).

Deletion of the hairpins (ΔH123), but not the β strands (Δβ), resulted in loss of CLSTN3β LD localization (Fig. 1g), indicating that the hydrophobic hairpins are the essential structural feature that facilitates LD targeting of CLSTN3β. Truncation mutants with only one or two hairpins were still able to localize to LDs, albeit with reduced efficiency (Extended Data Fig. 3g,h). Collectively, these results indicate that CLSTN3β localizes to ER–LD contact sites through the partitioning of its N-terminal hydrophobic hairpins onto LDs while its C-terminal transmembrane domain (shared with CLSTN3) remains anchored in the ER (Fig. 1h).

ER-localized CLSTN3β is degraded by ER-associated degradation

To explore mechanisms leading to enrichment of CLSTN3β at ER–LD contacts, we performed unbiased interactome analysis in brown adipocytes stably expressing CLSTN3β-APEX2-Flag. CLSTN3β-interacting proteins were isolated by (1) APEX2 proximity labelling[35] or (2) Flag immunoprecipitation. A resulting 287 proteins common to both datasets were considered high-confidence CLSTN3β binding partners (Extended Data Fig. 4a and Supplementary Data 2).

Gene ontology analysis revealed that components of the ER-associated degradation (ERAD) pathway were markedly overrepresented in the CLSTN3β interactome (Extended Data Fig. 4b). Previous studies have proposed that enrichment of membrane hairpin-containing proteins at

LDs is due to their conformational instability in the ER bilayer, leading to degradation of the ER fraction through ERAD[36–40]. Accordingly, we found that degradation of endogenous CLSTN3β in brown adipocytes was suppressed by the valosin-containing protein inhibitor CB-5083, implicating the ERAD pathway in CLSTN3β turnover (Extended Data Fig. 4c)[41]. Similarly, in untreated HeLa cells, CLSTN3β localized exclusively to small punctate structures, probably representing sites of LD biogenesis; however, in CB-5083-treated cells, CLSTN3β was visualized diffusely in ER not associated with LDs (Extended Data Fig. 4d).

Immunoprecipitation of CLSTN3β-Flag from human embryonic kidney 293T (HEK293T) cells cotransfected with HA-ubiquitin confirmed that CLSTN3β is modified with ubiquitin and that ubiquitinated CLSTN3β accumulates in cells treated with MG132 or CB-5083 (Extended Data Fig. 4e). Two conspicuous ERAD proteins in the CLSTN3β interactome were the E3 ligase autocrine motility factor receptor (AMFR)/gp78 and its cognate E2 UBE2G2 (Supplementary Data 2)[36,40,42]. We confirmed that gp78 and UBE2G2 associate with CLSTN3β in HEK293T cells (Extended Data Fig. 4f). Furthermore, gp78 overexpression reduced CLSTN3β protein and increased CLSTN3β ubiquitination, whereas gp78 knockdown enhanced CLSTN3β stability (Extended Data Fig. 4f,g). These results indicate that CLSTN3β concentrates at ER–LD contact sites in part because the ER fraction is degraded through a UBE2G2-gp78 ERAD pathway.

CLSTN3β knockout perturbs LD form and function

To determine the physiological function of CLSTN3β, we generated global and adipocyte-specific knockout (KO) mice (CLSTN3β KO and AdC3KO, respectively, Extended Data Fig. 5a–d). When housed under standard conditions (22 °C) and fed a standard chow diet, adult AdC3KO mice had larger and paler BAT than wild-type (WT) littermates, despite having similar body weight and composition (Fig. 2a and Extended Data Fig. 5e). Accordingly, both AdC3KO and CLSTN3β KO mice had increased BAT triglyceride content (Fig. 2b). Histologically, AdC3KO BAT had a markedly more unilocular appearance (Fig. 2c,d). AdC3KO mice were able to maintain euthermia during cold acclimation, although their BAT triglyceride content and LD size remained higher than WT mice (Extended Data Fig. 5f–i). However, when compensatory thermogenic mechanisms were first suppressed by pre-acclimating the mice to thermoneutrality, CLSTN3β-deficient mice became hypothermic at a faster rate than controls during acute cold challenge (Fig. 2e).

RNA-sequencing analysis of BAT before and after acute cold challenge revealed that the broad programme of cold-inducible genes was largely unchanged by loss of CLSTN3β (Fig. 2f). Induction of classical thermogenic genes in BAT and inguinal WAT (iWAT) with cold acclimation or rosiglitazone was also similar between genotypes, despite the fact that AdC3KO BAT and iWAT appeared to be less multilocular under these conditions (Extended Data Fig. 5j–l). Thus, loss of CLSTN3β causes a thermogenic defect that is not associated with broad changes in thermogenic gene expression.

As CLSTN3β localizes specifically to ER–LD contact sites, we hypothesized that its function in thermogenic adipocytes is to regulate lipid utilization. Consistent with this hypothesis, both AdC3KO and CLSTN3β KO mice had higher respiratory exchange ratios than their WT counterparts (Fig. 2g), indicating that they oxidized less lipid and more carbohydrate. To directly assess carbohydrate utilization in BAT, we measured ^{18}F-fluorodeoxyglucose (^{18}F-FDG) uptake during acute cold exposure by positron emission tomography with computed tomography (PET–CT). AdC3KO BAT accumulated on average 50% more ^{18}F-FDG compared to WT BAT (Fig. 2h,i). With respect to lipid use, LDs isolated from AdC3KO BAT had lower amounts of prolipolytic factors per unit triglyceride compared to LDs isolated from WT BAT (Extended Data Fig. 6a,b). We did not detect significant differences in basal or stimulated lipolysis in AdC3KO iWAT (Extended Data Fig. 6c), consistent with the low level of CLSTN3β expression in white adipocytes. When fed a HFD, AdC3KO and CLSTN3β KO mice accumulated more lipid in BAT, but maintained similar overall body weight and composition as WT mice (Extended Data Fig. 7a–d). Thus, whereas loss of CLSTN3β was not sufficient to perturb whole body energy balance under these conditions (Extended Data Fig. 7e), it induced a compensatory shift in substrate utilization away from lipid and towards carbohydrate, leading to increased lipid deposition in BAT.

CLSTN3β was recently reported to promote sympathetic innervation of thermogenic adipose tissue[26]. In our models, we observed no differences in adipose innervation on loss of CLSTN3β, as assessed by three-dimensional imaging of sympathetic nerve fibres in whole BAT lobes (Extended Data Fig. 8a–d and Supplementary Videos 1 and 2) and western blot analysis of tyrosine hydroxylase amounts in BAT and iWAT (Extended Data Fig. 8e–h). Downstream consequences of sympathetic activation, including phosphorylation of cAMP-dependent protein kinase substrates and UCP1 protein expression, were comparable in brown and beige fat from WT and CLSTN3β-deficient mice (Extended Data Fig. 8e–h). We conclude that sympathetic innervation and β-adrenergic signalling remain intact in our CLSTN3β loss-of-function models (Supplementary Discussion).

CLSTN3β promotes lipid utilization

We generated a CLSTN3β KO brown preadipocyte clone (Extended Data Fig. 9a) and stably expressed either mCherry or CLSTN3β-mCherry in this line. Differentiated CLSTN3β KO cells expressing mCherry had large LDs typical of cultured adipocytes; however, expression of CLSTN3β-mCherry resulted in an accentuated multilocular LD phenotype (Fig. 3a and Extended Data Fig. 9b). Re-expression of CLSTN3β markedly increased LD number and decreased LD size (Fig. 3a,b), producing adipocytes filled with 'grape-like' clusters of uniformly small LDs[43]. This phenotype appeared to be dose-dependent and was also observed in primary brown adipocytes (Fig. 3a,c).

Functionally, the multilocular LD phenotype of CLSTN3β-expressing adipocytes was associated with greater carbonyl cyanide 4-(trifluoromethoxy)phenylhydrazone- (FCCP)-induced mitochondrial respiration, attributable to more efficient lipolysis and fatty acid oxidation and not to increased mitochondrial content (Fig. 3d and Extended Data Fig. 9c,d). Accordingly, LDs isolated from CLSTN3β-expressing adipocytes had higher amounts of ATGL and CGI58 per unit triglyceride (Fig. 3e,f and Extended Data Fig. 9e), consistent with increased accessibility of the lipolytic machinery to an expanded LD surface area. These data indicate that CLSTN3β promotes multilocularity and lipid utilization in adipocytes through a cell-autonomous mechanism.

To determine whether CLSTN3β expression was sufficient to promote a multilocular LD phenotype in vivo, we expressed green fluorescent protein (GFP) or CLSTN3β in adipocytes of AdC3KO mice by intravenous AAV8-FLEX injection. Adult mice were administered adeno-associated virus (AAV), exposed to cold to minimize initial LD size and then housed at thermoneutrality to promote LD expansion. CLSTN3β-expressing mice maintained a greater degree of BAT multilocularity than GFP-expressing mice, even though adrenergic tone is minimal at thermoneutrality (Fig. 4a–d). These histological differences were not associated with changes in thermogenic gene expression or tyrosine hydroxylase amounts (Fig. 4e and Extended Data Fig. 9f). To replicate this effect in WAT, we injected AAV subcutaneously near the anterior subcutaneous WAT (asWAT) depot[44], stimulated beiging by prolonged cold exposure, and induced whitening by acclimation to thermoneutrality. While asWAT from GFP-expressing mice returned to a unilocular state after these manipulations, pockets of multilocular adipocytes persisted in asWAT from CLSTN3β-expressing mice (Fig. 4f and Extended Data Fig. 9g). Collectively, these results demonstrate that CLSTN3β can enforce a multilocular LD phenotype in both BAT and WAT.

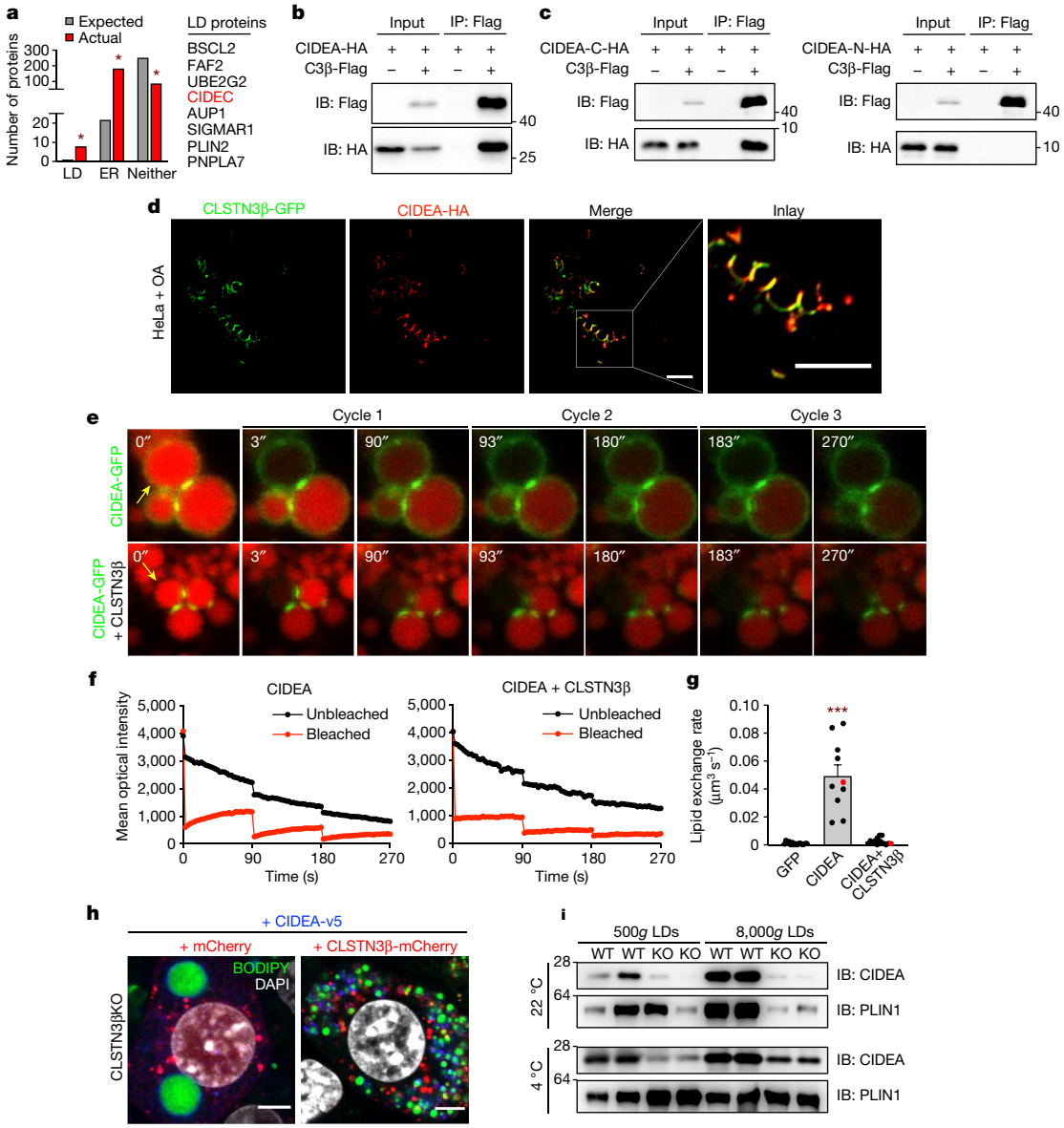

Fig. 5 | CLSTN3β associates with CIDE proteins and blocks LD fusion. **a**, Actual, number of proteins in the high-confidence CLSTN3β interactome with annotated LD, ER and neither localization in UniProt. Expected, number of proteins in a random sample of equal size from the UniProt mouse proteome with annotated LD, ER and neither localization. **b**, CLSTN3β-Flag and CIDEA-HA co-immunoprecipitation assay in transfected HEK293FT cells. **c**, CLSTN3β-Flag and HA-tagged CIDEA C-terminal region (CIDEA-C-HA) (left) or HA-tagged CIDEA N-terminal region (CIDEA-N-HA) (right) co-immunoprecipitation assay in transfected HEK293FT cells. **d**, Colocalization of CLSTN3β-GFP and CIDEA-HA in transfected HeLa cells treated with OA. Scale bar, 5 μm. **e**–**g**, FRAP-based lipid exchange rate assay in transfected 3T3-L1 preadipocytes incubated with 200 μM OA and 1 μg ml^{-1} BODIPY 558/568 C_{12} fatty acid for 16 h. **e**, Representative images of FRAP-based lipid exchange rate assay. Yellow arrows point to bleached LDs. **f**, Representative mean optical intensity traces for one pair of LDs from each group. **g**, Calculated lipid exchange rates (n = 15, 10, 14 cells). Cells used for representative traces are highlighted in red. **h**, Confocal microscopy of immortalized CLSTN3β KO brown adipocytes stably expressing mCherry or CLSTN3β-mCherry and CIDEA-v5 (day 5 of differentiation). Cells were stained with BODIPY 488, DAPI and anti-v5, and mCherry signal was amplified with anti-mCherry Alexa Fluor 594. Scale bar, 5 μm. **i**, BAT LDs isolated from female WT and AdC3KO mice housed at 22 or 4 °C for 24 h (n = 2 mice per lane). Equal amounts of TAG from each condition were loaded onto the gels. From the same experiment as Extended Data Fig. 6a,b. Bar plots show mean ± s.e.m. Each point represents a biological replicate. Two-sided *P < 0.001 by Fisher's exact test (**a**), ***P < 0.001 by ordinary one-way ANOVA with Tukey's multiple comparisons test (**g**).

CLSTN3β marks multilocular human fat

To examine the evolutionary conservation of *Clstn3b*, we performed a BLAST search for nucleotide sequences similar to the mouse *Clstn3b*-specific ORF (Supplementary Data 3). Consistent with a role for CLSTN3β in adipose thermogenesis, evolutionary conservation of *Clstn3b* is restricted to placental mammals (Extended Data Fig. 10a and Supplementary Data 4). One of the earliest organisms with a *Clstn3b* orthologue is the lesser hedgehog tenrec (*Echinops telfairi*), a phylogenetically ancient eutherian reported to be a 'protoendothermic' mammal[45]. Thus, whereas *Clstn3* is also found in non-mammalian vertebrates, *Clstn3b* has appeared more recently during evolution, coincident with the emergence of adipose thermogenesis as a homeostatic mechanism.

Visualization of RNA-sequencing reads mapping to the *CLSTN3* locus in human cerebral cortex and adipose tissue revealed a similar pattern of exon expression as in mouse tissues (Extended Data Fig. 10b). *CLSTN3* was previously identified as the most significantly enriched gene in

human multilocular versus unilocular adipose tissue[46,47]. To validate this finding, we analysed gene expression in periadrenal adipose tissue from control participants and patients with pheochromocytoma. *CLSTN3* expression was elevated in multilocular periadrenal fat from patients with pheochromocytoma[48], and quantitative PCR (qPCR) analysis confirmed that *CLSTN3* exons 17/18 and *CLSTN3B* were specifically enriched (Extended Data Fig. 10c,d).

We designed a custom RNAscope[49] probe set that targets the *CLSTN3B*-specific ORF and performed RNA in situ hybridization on a human adipose tissue microarray. We detected *CLSTN3B* RNA in multilocular fat from patients with pheochromocytoma but not in unilocular fat from control participants or patients with pheochromocytoma (Fig. 4g and Extended Data Fig. 10e). In the heterogeneous multilocular fat sections, *CLSTN3B* staining was restricted to nuclei from adipocytes with a multilocular morphology. Last, we generated a human multilocular fat cDNA library from a pheochromocytoma patient and cloned human CLSTN3β (Extended Data Fig. 10f). Like its mouse counterpart, human CLSTN3β readily localized to LDs in OA-loaded cells (Extended Data Fig. 10g,h).

CLSTN3β-CIDE association blocks LD fusion

The CLSTN3β interactome was markedly enriched for LD- and ER-localized proteins (Fig. 5a). Of the eight LD proteins in the interactome, CIDEC was of particular interest given the similarities between CLSTN3β gain-of-function and CIDE loss-of-function phenotypes. Specifically, accumulation of small, clustered LDs has also been observed with C-terminal mutations in CIDEs that impair their LD fusion capacity[6,11]. CLSTN3β coimmunoprecipitated with both CIDEA and CIDEC but not with RAB18 or CGI58 (Fig. 5b and Extended Data Fig. 11a–c). CLSTN3β interacted specifically with the C-terminal region of CIDEs (Fig. 5c and Extended Data Fig. 11d), which contains the LD-targeting amphipathic helix as well as residues critical for LD fusion[6,11,50]. In cells co-expressing CLSTN3β and CIDEA, CIDEA was still able to localize to LDs (Fig. 5d and Extended Data Fig. 11e), indicating that CLSTN3β does not interfere with CIDE-LD association. In fact, CLSTN3β appeared to colocalize with CIDEA at LD–LD contact sites where lipid transfer between LDs has been shown to occur[11,12].

We next measured CIDE lipid exchange rates in the presence or absence of CLSTN3β using a fluorescence recovery after photobleaching (FRAP)-based assay[11,12]. CIDEA- and CIDEC-dependent fluorescence recovery in the bleached LD was almost completely abolished when CLSTN3β was co-expressed (Fig. 5e–g, Extended Data Fig. 11f–h and Supplementary Video 3), indicating that CLSTN3β severely impairs CIDE-mediated lipid transfer. Consistent with this observation, CLSTN3β enforced a multilocular LD phenotype in HeLa cells expressing CIDEC (Extended Data Fig. 12a) and in brown adipocytes overexpressing CIDEs (Fig. 5h and Extended Data Fig. 12b). In BAT, loss of CLSTN3β was associated with a reduction in total and LD-associated CIDEA (Fig. 5i and Extended Data Fig. 12c), possibly as a compensatory response to enhanced CIDE lipid transfer activity and reduced LD surface area. CLSTN3β did not affect the ability of CIDEs to phase separate and form gel-like condensates (Extended Data Fig. 12d–f), which we have previously shown is mediated by the N-terminal region of CIDEs[13]. Collectively, these data show that CLSTN3β promotes multilocularity by associating with CIDEs and blocking their ability to transfer lipids at LD–LD contact sites and thereby facilitate LD fusion.

Discussion

Multilocularity is a defining characteristic of thermogenic adipocytes, but how this phenotype is acquired and maintained is largely unknown. Here, we have shown that the distinct multilocular morphology of thermogenic adipocytes is established through the action of CLSTN3β. CLSTN3β localizes to ER–LD contact sites, at which it limits LD expansion by blocking CIDE-mediated LD fusion. Gain- and loss-of-function studies revealed that CLSTN3β is necessary and sufficient to enforce a multilocular LD phenotype in cultured cells and adipose tissue. Mice lacking CLSTN3β manifest defects in cold tolerance and lipid metabolism, pointing to an important functional role for LD morphology in triglyceride utilization and thermogenesis. Future studies will delineate the biophysical mechanism by which CLSTN3β regulates CIDE lipid transfer activity. Plausible mechanisms include modulating the lipid permeability or internal organization of CIDE fusion plates, regulating the abundance of specific phospholipid species on the LD monolayer and recruiting ER-resident proteins to LDs to modify CIDE function. Other binding partners at ER–LD contact sites may also play important roles in mediating CLSTN3β function.

Adipose thermogenesis has consistently been shown to have profound anti-obesity and antidiabetic effects in mice, but whether this process can be targeted pharmacologically to alleviate the metabolic syndrome in humans remains unclear[51–55]. One main barrier to clinical translation is the fact that humans live primarily in thermoneutral environments, leading to gradual loss of multilocular adipocytes and mitochondrial mass in BAT[56–58]. We showed that *CLSTN3B* is associated with multilocular adipocytes in human fat. A recent study identified an intronic single-nucleotide polymorphism in *CLSTN3*, corresponding to a missense mutation in the LD-targeting domain of CLSTN3β, that is associated with systemic metabolic traits in humans[59]. In mice, we found that sustaining CLSTN3β amounts in thermogenic fat by AAV slowed the loss of multilocular adipocytes at thermoneutrality. The ability to maintain adipocyte multilocularity in human BAT under thermoneutral conditions may provide further opportunities to harness the power of adipose thermogenesis for therapy.

Online content

Any methods, additional references, Nature Portfolio reporting summaries, source data, extended data, supplementary information, acknowledgements, peer review information; details of author contributions and competing interests; and statements of data and code availability are available at https://doi.org/10.1038/s41586-022-05507-1.

1. Wang, W. & Seale, P. Control of brown and beige fat development. *Nat. Rev. Mol. Cell Biol.* **17**, 691–702 (2016).
2. Cohen, P. & Kajimura, S. The cellular and functional complexity of thermogenic fat. *Nat. Rev. Mol. Cell Biol.* **22**, 393–409 (2021).
3. Trayhurn, P. Brown adipose tissue—a therapeutic target in obesity? *Front. Physiol.* **9**, 1672 (2018).
4. Cannon, B. & Nedergaard, J. Brown adipose tissue: function and physiological significance. *Physiol. Rev.* **84**, 277–359 (2004).
5. Rasmussen, A. T. The so-called hibernating gland. *J. Morphol.* **38**, 147–205 (1923).
6. Barneda, D. et al. The brown adipocyte protein CIDEA promotes lipid droplet fusion via a phosphatidic acid-binding amphipathic helix. *eLife* **4**, e07485 (2015).
7. Nishimoto, Y. & Tamori, Y. CIDE family-mediated unique lipid droplet morphology in white adipose tissue and brown adipose tissue determines the adipocyte energy metabolism. *J. Atherosclerosis Thrombosis* **24**, 989–998 (2017).
8. Xu, L., Zhou, L. & Li, P. CIDE proteins and lipid metabolism. *Arter. Thromb. Vasc. Biol.* **32**, 1094–1098 (2012).
9. Gao, G. et al. Control of lipid droplet fusion and growth by CIDE family proteins. *Biochim. Biophys. Acta Mol. Cell Biol. Lipids* **1862**, 1197–1204 (2017).
10. Puri, V. et al. Cidea is associated with lipid droplets and insulin sensitivity in humans. *Proc. Natl Acad. Sci. USA* **105**, 7833–7838 (2008).
11. Gong, J. et al. Fsp27 promotes lipid droplet growth by lipid exchange and transfer at lipid droplet contact sites. *J. Cell Biol.* **195**, 953–963 (2011).
12. Sun, Z. et al. Perilipin1 promotes unilocular lipid droplet formation through the activation of Fsp27 in adipocytes. *Nat. Commun.* **4**, 1594 (2013).
13. Lyu, X. et al. A gel-like condensation of Cidec generates lipid-permeable plates for lipid droplet fusion. *Dev. Cell* **56**, 2592–2606.e7 (2021).
14. Zhou, Z. et al. Cidea-deficient mice have lean phenotype and are resistant to obesity. *Nat. Genet.* **35**, 49–56 (2003).
15. Nishimoto, Y. et al. Cell death-inducing DNA fragmentation factor A-like effector A and fat-specific protein 27β coordinately control lipid droplet size in brown adipocytes. *J. Biol. Chem.* **292**, 10824–10834 (2017).
16. Li, J. Z. et al. Cideb regulates diet-induced obesity, liver steatosis, and insulin sensitivity by controlling lipogenesis and fatty acid oxidation. *Diabetes* **56**, 2523–2532 (2007).

17. Zhou, L. et al. Cidea promotes hepatic steatosis by sensing dietary fatty acids. *Hepatology* **56**, 95–107 (2012).
18. Xu, X., Park, J. G., So, J. S. & Lee, A. H. Transcriptional activation of Fsp27 by the liver-enriched transcription factor CREBH promotes lipid droplet growth and hepatic steatosis. *Hepatology* **61**, 857–869 (2015).
19. Puri, V. et al. Fat-specific protein 27, a novel lipid droplet protein that enhances triglyceride storage. *J. Biol. Chem.* **282**, 34213–34218 (2007).
20. Nishino, N. et al. FSP27 contributes to efficient energy storage in murine white adipocytes by promoting the formation of unilocular lipid droplets. *J. Clin. Invest.* **118**, 2808–2821 (2008).
21. Toh, S. Y. et al. Up-regulation of mitochondrial activity and acquirement of brown adipose tissue-like property in the white adipose tissue of Fsp27 deficient mice. *PLoS ONE* **3**, e2890 (2008).
22. Rubio-Cabezas, O. et al. Partial lipodystrophy and insulin resistant diabetes in a patient with a homozygous nonsense mutation in CIDEC. *EMBO Mol. Med.* **1**, 280–287 (2009).
23. Ye, J. et al. Cideb, an ER- and lipid droplet-associated protein, mediates VLDL lipidation and maturation by interacting with apolipoprotein B. *Cell Metab.* **9**, 177–190 (2009).
24. Wu, L. Z. et al. Cidea controls lipid droplet fusion and lipid storage in brown and white adipose tissue. *Sci. China Life Sci.* **57**, 107–116 (2014).
25. Zhang, S. et al. Cidea control of lipid storage and secretion in mouse and human sebaceous glands. *Mol. Cell. Biol.* **34**, 1827–1838 (2014).
26. Zeng, X. et al. Innervation of thermogenic adipose tissue via a calsyntenin 3β–S100b axis. *Nature* **569**, 229–235 (2019).
27. Li, Y. I. et al. Annotation-free quantification of RNA splicing using LeafCutter. *Nat. Genet.* **50**, 151–158 (2018).
28. Siersbæk, M. S. et al. Genome-wide profiling of peroxisome proliferator-activated receptor γ in primary epididymal, inguinal, and brown adipocytes reveals depot-selective binding correlated with gene expression. *Mol. Cell. Biol.* **32**, 3452–3463 (2012).
29. Martell, J. D., Deerinck, T. J., Lam, S. S., Ellisman, M. H. & Ting, A. Y. Electron microscopy using the genetically encoded APEX2 tag in cultured mammalian cells. *Nat. Protoc.* **12**, 1792–1816 (2017).
30. Krogh, A., Larsson, B., Von Heijne, G. & Sonnhammer, E. L. L. Predicting transmembrane protein topology with a hidden Markov model: Application to complete genomes. *J. Mol. Biol.* **305**, 567–580 (2001).
31. Yang, J. & Zhang, Y. I-TASSER server: New development for protein structure and function predictions. *Nucleic Acids Res.* **43**, W174–W181 (2015).
32. Buchan, D. W. A. & Jones, D. T. The PSIPRED Protein Analysis Workbench: 20 years on. *Nucleic Acids Res.* **47**, W402–W407 (2019).
33. Källberg, M. et al. Template-based protein structure modeling using the RaptorX web server. *Nat. Protoc.* **7**, 1511–1522 (2012).
34. Baek, M. et al. Accurate prediction of protein structures and interactions using a three-track neural network. *Science (80-.).* **373**, 871–876 (2021).
35. Hung, V. et al. Spatially resolved proteomic mapping in living cells with the engineered peroxidase APEX2. *Nat. Protoc.* **11**, 456–475 (2016).
36. Stevenson, J., Huang, E. Y. & Olzmann, J. A. Endoplasmic reticulum-associated degradation and lipid homeostasis. *Annual Rev. Nutrition* **36**, 511–542 (2016).
37. Olzmann, J. A. & Carvalho, P. Dynamics and functions of lipid droplets. *Nat. Rev. Mol. Cell Biol.* **20**, 137–155 (2019).
38. Roberts, M. A. & Olzmann, J. A. Protein quality control and lipid droplet metabolism. *Annu. Rev. Cell Dev. Biol.* **36**, 115–139 (2020).
39. Ruggiano, A., Mora, G., Buxó, L. & Carvalho, P. Spatial control of lipid droplet proteins by the ERAD ubiquitin ligase Doa10. *EMBO J.* **35**, 1644–1655 (2016).
40. Bersuker, K. et al. A proximity labeling strategy provides insights into the composition and dynamics of lipid droplet proteomes. *Dev. Cell* **44**, 97–112.e7 (2018).
41. Huang, E. Y. et al. A VCP inhibitor substrate trapping approach (VISTA) enables proteomic profiling of endogenous ERAD substrates. *Mol. Biol. Cell* **29**, 1021–1030 (2018).
42. Song, B. L., Sever, N. & DeBose-Boyd, R. A. Gp78, a membrane-anchored ubiquitin ligase, associates with Insig-1 and couples sterol-regulated ubiquitination to degradation of HMG CoA reductase. *Mol. Cell* **19**, 829–840 (2005).
43. Guo, Y. et al. Functional genomic screen reveals genes involved in lipid-droplet formation and utilization. *Nature* **453**, 657–661 (2008).
44. Bagchi, D. P., Forss, I., Mandrup, S. & MacDougald, O. A. SnapShot: niche determines adipocyte character I. *Cell Metabolism* **27**, 264–264.e1 (2018).
45. Oelkrug, R. et al. Brown fat in a protoendothermic mammal fuels eutherian evolution. *Nat. Commun.* **4**, 2140 (2013).
46. Jespersen, N. Z. et al. Heterogeneity in the perirenal region of humans suggests presence of dormant brown adipose tissue that contains brown fat precursor cells. *Mol. Metab.* **24**, 30–43 (2019).
47. Plucińska, K. et al. Calsyntenin 3β is dynamically regulated by temperature in murine brown adipose and marks human multilocular fat. *Front. Endocrinol.* **11**, 767 (2020).
48. Vergnes, L. et al. Adipocyte browning and higher mitochondrial function in periadrenal but not SC fat in pheochromocytoma. *J. Clin. Endocrinol. Metab.* **101**, 4440–4448 (2016).
49. Wang, F. et al. RNAscope: a novel in situ RNA analysis platform for formalin-fixed, paraffin-embedded tissues. *J. Mol. Diagnostics* **14**, 22–29 (2012).
50. Christianson, J. L., Boutet, E., Puri, V., Chawla, A. & Czech, M. P. Identification of the lipid droplet targeting domain of the Cidea protein. *J. Lipid Res.* **51**, 3455–3462 (2010).
51. Cypess, A. M. et al. Identification and importance of brown adipose tissue in adult humans. *N. Engl. J. Med.* **360**, 1509–1517 (2009).
52. van Marken Lichtenbelt, W. D. et al. Cold-activated brown adipose tissue in healthy men. *N. Engl. J. Med.* **360**, 1500–1508 (2009).
53. Virtanen, K. A. et al. Functional brown adipose tissue in healthy adults. *N. Engl. J. Med.* **360**, 1518–1525 (2009).
54. Cypess, A. M. et al. Activation of human brown adipose tissue by a β3-adrenergic receptor agonist. *Cell Metab.* **21**, 33–38 (2015).
55. Becher, T. et al. Brown adipose tissue is associated with cardiometabolic health. *Nat. Med.* **27**, 58–65 (2021).
56. de Jong, J. M. A. et al. Human brown adipose tissue is phenocopied by classical brown adipose tissue in physiologically humanized mice. *Nat. Metab.* **1**, 830–843 (2019).
57. Sass, F. et al. TFEB deficiency attenuates mitochondrial degradation upon brown adipose tissue whitening at thermoneutrality. *Mol. Metab.* **47**, 101173 (2021).
58. Schlein, C. et al. Endogenous fatty acid synthesis drives brown adipose tissue involution. *Cell Rep.* **34**, 108624 (2021).
59. Bai, N. et al. CLSTN3 gene variant associates with obesity risk and contributes to dysfunction in white adipose tissue. *Mol. Metab.* **63**, 101531 (2022).

Methods

Clstn3b transcript annotation

Brown adipocyte RNA and assay for transposase-accessible chromatin-sequencing data were previously published by our laboratory[60]. Adipocyte CAGE-sequencing data were obtained from the Functional Annotation of the Mammalian Genome project. Cortex and BAT RNA and ChIP-sequencing data were obtained from the Encyclopedia of DNA Elements project. Cortex and BAT RNA-sequencing data for LeafCutter splicing analysis were obtained from GSE65776.

The 5′ RLM-RACE was performed on total RNA from mouse BAT using the FirstChoice RLM-RACE Kit (Ambion). RACE products were Gateway cloned into the pDONR221 vector and inserts were Sanger sequenced. Ten colonies per RACE product were sequenced to survey the distribution of transcription start sites. RACE primers can be found in Supplementary Table 1.

RT–PCR was performed on total RNA from mouse BAT using KOD Hot Start DNA Polymerase (Millipore). RNA was depleted of genomic DNA using RNeasy Plus Mini Kit guide DNA Eliminator columns (Qiagen) and DNase I (NEB). RT–PCR primers can be found in Supplementary Table 1.

Immortalized brown preadipocytes

Primary mouse brown preadipocytes were isolated and immortalized as previously described by our laboratory[60]. Single cell clones were generated by limiting dilution and clones with high expression of *Clstn3* and *Ucp1* after differentiation without/with isoproterenol stimulation were selected for further studies. Adipocyte differentiation was initiated by culturing the cells for 2 d in 1.25 μM dexamethasone, 0.5 mM isobutylmethylxanthine, 125 μM indomethacin, 4 mg ml^{-1} insulin, 1 μM rosiglitazone and 2 nM T3 in DMEM plus 10% FBS, 1% P/S and GlutaMAX (Gibco). Cells were then maintained in 4 mg ml^{-1} insulin, 1 μM rosiglitazone and 2 nM T3 in DMEM plus 10% FBS, 1% P/S and GlutaMAX until collection.

To generate CLSTN3β KO pools and clones, brown preadipocyte clones were transfected with guide RNA–Cas9-GFP constructs (PX458, Addgene plasmid no. 48138) and GFP^+ cells were selected by fluorescence-activated cell sorting. After a recovery period, genome editing efficiency was determined by PCR amplification of genomic DNA followed by Sanger sequencing and tracking of indels by decomposition analysis[61]. As needed, single cell clones were generated by limiting dilution and KO clones were identified by PCR amplification of genomic DNA followed by Sanger sequencing and CRISP-ID analysis[62]. Guide RNA sequences can be found in Supplementary Table 1.

Plasmids were stably expressed in brown preadipocyte clones by lentiviral transduction. Crude lentivirus was produced in HEK293T cells and transduced preadipocytes were selected with puromycin and/or blasticidin.

Western blot

Unless otherwise indicated, whole cell and tissue lysates were prepared using RIPA buffer (Boston BioProducts) supplemented with protease and phosphatase inhibitor cocktails (Roche). Protein concentrations were measured using the BCA Protein Assay Kit (Pierce). Equal amounts of protein were loaded onto NuPAGE 4–12% Bis-Tris gels (Invitrogen) and transferred to Amersham Hybond P 0.45 μm polyvinyl difluoride membranes (Cytiva). Membranes were blocked for 1 h at room temperature with 5% milk or 3% bovine serum albumin (BSA) in TBS + 0.1% Tween 20 (TBST). Primary antibodies were diluted in 3% BSA in TBST and incubated with membranes overnight at 4 °C. Membranes were then washed three times with TBST at room temperature for 10 min per wash. Secondary antibodies were diluted in 5% milk or 3% BSA in TBST and incubated with membranes for 1 h at room temperature. After three more TBST washes, membranes were developed for 5 min at room temperature using Immobilon Forte Western horseradish peroxidase substrate (Millipore). Western blots were imaged using the Syngene PXi gel documentation system. Quantification of band intensities was performed using ImageJ (NIH). Gel source data can be found in Supplementary Fig. 1.

The following primary antibodies were used for western blot: ATGL (30A4), Cell Signaling no. 2439 (1:1,000); Calnexin, Abcam ab10286 (1:1,000); Calreticulin (D3E6), Cell Signaling no. 12238 (1:1,000); CGI58 (EPR12621), Abcam ab183739 (1:1,000); CIDEA, Proteintech 13170-1-AP (1:1,000); CLSTN3, Proteintech 13302-1-AP (1:1,000); FABP4 (B-4), Santa Cruz sc-271529 (1:5,000); Flag (M2), MilliporeSigma F1804 (1:2,000); gp78/AMFR, Cell Signaling no. 9590 (1:1,000); GRP94 (9G10), Thermo Fisher MA3-016 (1:1,000); HA (C29F4), Cell Signaling no. 3724 (1:1,000); HSL, Cell Signaling no. 4107 (1:2,000); Myc (4A6), MilliporeSigma 05-724 (1:1,000); OXPHOS, Abcam ab110413 (1:5,000); p-HSL S563, Cell Signaling no. 4139 (1:1,000); p-HSL S660, Cell Signaling no. 4126 (1:1,000); PLIN1 (D1D8), Cell Signaling no. 9349 (1:1,000); PLIN2 (EPR3713), Abcam ab108323 (1:1,000); p-cAMP-dependent protein kinase substrate (100G7E), Cell Signaling no. 9624 (1:1,000); S100B (EP1576Y), Abcam ab52642 (1:1,000); S6 (54D2), Cell Signaling no. 2317 (1:1,000); TH (LNC1), MilliporeSigma MAB318 (1:1,000); TIMM23, Proteintech 11123-1-AP (1:1,000); TOMM20, Proteintech 11802-1-AP (1:1,000); Ubiquitin, Proteintech 10201-2-AP (1:1,000); UCP1, Abcam ab10983 (1:5,000); β-Actin, MilliporeSigma A2066 (1:2,000) and β-Tubulin, Abcam ab15568 (1:2,000).

For membrane isolation, cells and tissues were resuspended and homogenized in DS buffer (50 mM Tris-HCl pH 7.4, 150 mM NaCl, 1.25 mM EDTA, 1.5 mM DTT, protease inhibitors) and lysed by sonication (Misonix Sonicator 3000, five cycles, 3 s on, 15 s off, output level 3). Nuclei and unbroken cells were pelleted by centrifuging at 2,000*g* for 5 min at 4 °C. Membranes were pelleted by centrifuging the post-nuclear supernatant at 100,000*g* for 45 min at 4 °C. Membrane pellets were resuspended in DS buffer using a 100 μl Hamilton syringe. Protein concentrations were measured using the 660 nm Protein Assay Reagent (Pierce) and western blots were performed as described above.

Immunoprecipitation (for MS/MS analysis)

For immunoprecipitation of endogenous CLSTN3β, immortalized brown preadipocytes were differentiated for 5 days, washed twice with ice-cold PBS and incubated with lysis buffer (50 mM Tris-HCl pH 7.4, 150 mM NaCl, 1% NP-40 substitute, 0.5% sodium deoxycholate, protease inhibitors) for 30 min on ice. Lysates were cleared by centrifuging at 12,000*g* for 15 min at 4 °C. Supernatants were retained and protein concentrations were measured using the BCA Protein Assay Kit (Pierce). Lysates were incubated with anti-CLSTN3 antibody (13302-1-AP, Proteintech, 1:100) with end-over-end rotation for 1 h at 4 °C, followed by incubation with protein A/G beads (sc-2003, Santa Cruz) with end-over-end rotation overnight at 4 °C. Beads were washed five times for 20 min per wash with end-over-end rotation at 4 °C: twice with lysis buffer, twice with high salt wash buffer (50 mM Tris-HCl pH 7.4, 500 mM NaCl, 0.1% NP-40 substitute, 0.05% sodium deoxycholate) and once with low salt wash buffer (10 mM Tris-HCl pH 7.4, 0.1% NP-40 substitute, 0.05% sodium deoxycholate). For western blot analysis, proteins were eluted from beads using 0.2 M glycine pH 2.6 and neutralized using Tris pH 8.0.

For MS/MS analysis, proteins were eluted from beads by heating (95 °C, 5 min) in lysis buffer (100 μl, 12 mM sodium lauroyl sarcosine, 0.5% sodium deoxycholate, 50 mM triethylammonium bicarbonate (TEAB), Halt Protease and Phosphatase Inhibitor Cocktail (Thermo Fisher Scientific)). The samples were treated with Tris(2-carboxyethyl) phosphine (10 μl, 55 mM in 50 mM TEAB, 30 min, 60 °C), followed by chloroacetamide (10 μl, 120 mM in 50 mM TEAB, 30 min, 25 °C in the dark). They were then diluted fivefold with aqueous 50 mM TEAB and incubated overnight with Sequencing Grade Modified Trypsin (1 μg in 10 μl of 50 mM TEAB; Promega). Following this, an equal volume of ethyl acetate:trifluoroacetic acid (TFA) (100:1, v/v) was added, and

after vigorous mixing (5 min) and centrifugation (13,000*g*, 5 min), the supernatants were discarded and the lower phases were dried in a centrifugal vacuum concentrator. The samples were then desalted using a modified version of Rappsilber's protocol in which the dried samples were reconstituted in acetonitrile:water:TFA (solvent A, 100 µl, 2:98:0.1, v/v/v) and then loaded onto a small portion of a C18-silica disc (3M) placed in a 200 µl pipette tip. Before sample loading, the C18 disc was prepared by sequential treatment with methanol (20 µl), acetonitrile:water:TFA (solvent B, 20 µl, 80:20:0.1, v/v/v) and finally solvent A (20 µl). After loading the sample, the disc was washed with solvent A (20 µl, eluent discarded) and eluted with solvent B (40 µl). The collected eluent was dried in a centrifugal vacuum concentrator and reconstituted in water:acetonitrile:FA (solvent E, 10 µl, 98:2:0.1, v/v/v). Aliquots (5 µl) were injected onto a reverse phase nanobore high-performance liquid chromatography column (AcuTech Scientific, C18, 1.8 µm particle size, 360 µm × 20 cm, 150 µm ID), equilibrated in solvent E and eluted (500 nl min^{-1}) with an increasing concentration of solvent F (acetonitrile:water:FA, 98:2:0.1, v/v/v; min:%F: 0:0, 5:3, 18:7, 74:12, 144:24, 153:27, 162:40, 164:80, 174:80, 176:0, 180:0) using an Eksigent NanoLC-2D system (Sciex). The effluent from the column was directed to a nanospray ionization source connected to a hybrid quadrupole-Orbitrap mass spectrometer (Q Exactive Plus, Thermo Fisher Scientific) acquiring mass spectra in a data-dependent mode alternating between a full scan (*m/z* 350–1,700, automated gain control target 3 × 106, 50 ms maximum injection time, full-width at half-maximum resolution 70,000 at *m/z* 200) and up to 15 MS/MS scans (quadrupole isolation of charge states 2–7, isolation window 0.7 *m/z*) with previously optimized fragmentation conditions (normalized collision energy of 32, dynamic exclusion of 30 s, automated gain control target 1 × 105, 100 ms maximum injection time, full-width at half-maximum resolution 35,000 at *m/z* 200). The raw data were analysed in Mascot Daemon (Matrix Science), which provided measurements of abundance for the identified peptides. Tryptic peptides containing amino acid sequences unique to individual proteins were used to identify proteins in each sample. The putative sequence for CLSTN3β was included in the database search and was used to identify a peptide from the unknown region (SAAVEVGRPQGETPQEQQPCR, mass accuracy −1.03 ppm, expected value 0.00023), as well as a peptide from the known region (IIESPPHRY, mass accuracy −0.53 ppm, expected value 0.0059).

Gene expression analysis

For qPCR, total RNA was extracted using TRIzol reagent (Invitrogen) and reverse transcribed. cDNA was amplified and quantified using iTaq Universal SYBR Green Supermix (Bio-Rad) and the QuantStudio 6 Flex 384-well qPCR system (Applied Biosystems). Relative expression levels were calculated using standard curves, and expression of housekeeping genes (primarily *36b4*) was used for normalization. qPCR primers can be found in Supplementary Table 1.

For RNA sequencing, total RNA was extracted using TRIzol and the RNeasy Mini Kit with on-column DNase I digestion (Qiagen). Library preparation and sequencing were done at GENEWIZ. Adapter and quality trimming of raw FASTQ files was performed using Trimmomatic. FastQC was used to analyse FASTQ files before and after trimming. Trimmed FASTQ files were aligned to GRCm38/mm10 using STAR. HTSeq-count was used to extract gene counts and differential gene expression analysis was carried out using DESeq2.

ChIP

Differentiated C3H/10T1/2 cells were crosslinked with 1% formaldehyde for 10 min and quenched with glycine (final concentration 125 mM). Cells were then lysed in AF buffer (50 mM Tris pH 8, 5 mM EDTA, 1% SDS, protease inhibitors) and sonicated using a Bioruptor Pico (Diagenode, ten cycles, 10 s on, 30 s off). Sheared chromatin was immunoprecipitated by overnight incubation with normal rabbit IgG (no. 2729, Cell Signaling, 1:100) or anti-PPARγ antibody (no. 2443, Cell Signaling, 1:100), and antibody–chromatin complexes were captured by a 4-h incubation with protein A/G beads (sc-2003, Santa Cruz). Immunoprecipitated and input chromatin was de-crosslinked overnight and purified by phenol-chloroform extraction and ethanol precipitation. Chromatin samples were then analysed by qPCR. All data were normalized to input DNA. ChIP–qPCR primers can be found in Supplementary Table 1.

APEX2 electron microscopy

Immortalized brown preadipocytes stably expressing CLSTN3β-APEX2 were prepared for electron microscopy as described previously[29]. Briefly, brown preadipocytes were plated on 35 mm glass-bottom dishes (P35GC-1.5-14-C, MatTek) and were left untreated, treated with 1 mM OA for 2 h or differentiated for 4 days. Culture medium was aspirated and cells were prefixed in freshly prepared 2% glutaraldehyde in cacodylate buffer (100 mM sodium cacodylate, 2 mM $CaCl_2$, pH 7.4) at room temperature. Glutaraldehyde was aspirated and replaced with fresh 2% glutaraldehyde in cacodylate buffer, and dishes were placed on ice for 60 min. Cells were then washed five times in ice-cold cacodylate buffer, 2–5 min per wash. Glutaraldehyde was quenched with 30 mM glycine in cacodylate buffer for 5 min on ice, and cells were washed again five times in ice-cold cacodylate buffer. Cells were incubated with freshly prepared 3,3′-diaminobenzidine (DAB) solution (0.4 mg ml^{-1} DAB free base, 10 mM H_2O_2, pH 7.2 in cacodylate buffer) for 5–15 min on ice, followed by five more washes in ice-cold cacodylate buffer.

After washing with cacodylate buffer, the samples were incubated with 2% osmium tetroxide, 1.5% potassium ferricyanide in 0.1 M sodium cacodylate for 1 h. Next, the samples were washed five times (5 min each) with deionized water, then incubated with 2% uranyl acetate in the fridge overnight. The following day, the samples were washed five times (5 min each) with deionized water, then the glass coverslips were detached from the dishes with the coverslip removal fluid (MatTek) and transferred into individual glass jars. The cells were then dehydrated through a series of increasing ethanol concentrations (30, 50, 70, 80, 95, 100%), 3 min each. The samples were incubated with 100% ethanol twice more for 3 min each. Samples were then infiltrated with EMbed 812 by incubation with 1:1 EMbed 812:acetone for 30 min, then 2:1 EMbed 812:acetone overnight. The next day, the samples were incubated in freshly prepared EMbed 812 (100%) for 2 h. Next, the coverslips were held vertically with forceps to allow all of the excess resin to drip off, the back was wiped with a Kimwipe and the coverslip was placed (cell-side down) onto a BEEM capsule, which was filled to the top with fresh EMbed 812 resin. Samples were allowed to polymerize in a 60 °C oven for 48 h. To remove the glass coverslip from the polymerized block, leaving the embedded cells behind, samples were quickly transferred repeatedly between a dewar filled with liquid nitrogen and a beaker filled with 60 °C water. The block was then placed into a holder for trimming and sectioning with a Leica UC6 ultramicrotome. Next, 65 nm sections were collected onto freshly glow-discharged copper grids and then stained with Reynold's lead citrate. Transmission electron micrographs were collected at the California NanoSystems Institute at UCLA.

Immunofluorescence

HeLa cells were plated in a standard 12-well format, with each well containing a poly-D-lysine-coated glass coverslip (GG-12-1.5PDL, Neuvitro). Immortalized brown preadipocytes were differentiated in 35-mm glass-bottom dishes (P35GC-1.5-14-C, MatTek). Primary brown preadipocytes were first differentiated in a standard six-well format; 1 d before processing, cells were replated in a standard 12-well format, with each well containing a poly-D-lysine-coated glass coverslip.

Cells were rinsed once with room temperature PBS, fixed with 4% paraformaldehyde in PBS for 10–30 min at room temperature and

then rinsed three times with ice-cold PBS. Cells were permeabilized with 100 μM digitonin in PBS for 10 min at room temperature and then washed three times with PBS for 5 min per wash. Cells were blocked with 1% BSA, 0.3 M glycine in PBS + 0.1% Tween 20 (PBST) for 30 min at room temperature and then incubated with primary antibody diluted in 1% BSA in PBST overnight at 4 °C. Cells were washed three times with PBS, 5 min per wash, incubated with secondary antibody diluted in 1% BSA in PBS for 1 h at room temperature and then washed three more times with PBS for 5 min per wash. LDs were stained by incubation with 1–5 μg ml^{-1} BODIPY 488 or LipidTOX 647 (1:1,000) in PBS for 30–60 min at room temperature, followed by three PBS rinses. Coverslips were mounted onto microscope slides using ProLong Gold Antifade Mountant with DAPI (4,6-diamidino-2-phenylindole) (Invitrogen).

The following primary antibodies were used for immunofluorescence: Flag (M2), MilliporeSigma F1804 (1:500); HA (C29F4), Cell Signaling no. 3724 (1:500); mCherry AF594 (16D7), Thermo Fisher M11240 (1:1,000) and V5, Cell Signaling no. 13202 (1:500).

Confocal microscopy was performed using a Leica SP8 confocal microscope housed at the California NanoSystems Institute at UCLA. Images were prepared using ImageJ (NIH).

Biochemical extraction of membrane proteins

Transfected HEK293T cells were collected by scraping into PBS, pelleted by centrifugation and resuspended in HB1 buffer (20 mM HEPES-KOH pH 7.4, 400 mM sucrose, 1 mM EDTA, 0.3 mM DTT, protease and phosphatase inhibitors). Cells were lysed by passaging them 20 times through a 23G needle. Postnuclear supernatant was retained after centrifugation at 1,000*g* for 10 min at 4 °C, divided into three equal volumes and centrifuged at 25,000*g* for 10 min at 4 °C to pellet membranes. The three membrane pellets were resuspended in the following solutions plus protease inhibitors: (1) standard buffer (50 mM Tris-HCl pH 7.4, 150 mM NaCl), (2) high pH solution (0.1 M Na_2CO_3, 150 mM NaCl) and (3) high salt buffer (50 mM Tris-HCl pH 7.4, 1 M NaCl). After centrifuging again at 25,000*g* for 10 min at 4 °C, supernatants were retained and pellets were resuspended in the same three solutions. Samples were subsequently analysed by western blot.

Protease protection assay

Transfected HEK293T cells were collected by scraping into PBS, pelleted by centrifugation and resuspended in HB1 buffer (20 mM HEPES-KOH pH 7.4, 400 mM sucrose, 1 mM EDTA, 0.3 mM DTT, protease and phosphatase inhibitors). Cells were lysed by passaging them 20 times through a 23G needle. Nuclei and unbroken cells were pelleted by centrifuging at 1,000*g* for 10 min at 4 °C, and postnuclear supernatant was centrifuged at 25,000*g* for 10 min at 4 °C to pellet membranes. Each membrane pellet was washed and resuspended in B88 buffer (20 mM HEPES-KOH pH 7.4, 250 mM sorbitol, 150 mM KAc, 5 mM $MgAc_2$) and then divided into three equal volumes. The three reactions were set up as follows: (1) no treatment, (2) trypsin (Sigma, 12.5 μg ml^{-1}) and (3) 1% Triton X-100 for 15 min on ice, then trypsin (12.5 μg ml^{-1}). All three reactions were incubated for 15 min at 30 °C followed by 15 min on ice. The reactions were stopped by treating with trypsin inhibitor (Sigma, 50 μg ml^{-1}) for 5 min at room temperature followed by 5 min on ice. Samples were subsequently analysed by western blot.

CLSTN3β interactome analysis

APEX2 proximity labelling was performed as described previously[35]. Briefly, immortalized brown preadipocytes stably expressing CLSTN3β-APEX2-Flag were differentiated for 4 d and stimulated with vehicle or isoproterenol (10 μM, 2 h). Cells were treated with 500 μM biotin-phenol (Iris Biotech) for 45 min at 37 °C, followed by 1 mM H_2O_2 for 1 min at room temperature. Cells were washed five times according to the published protocol, scraped into fresh quencher solution, pelleted by centrifugation, flash-frozen in liquid nitrogen and stored at −80 °C.

Thawed cell pellets were resuspended in a buffer containing 50 mM Tris-HCl pH 7.4, 150 mM NaCl, protease and phosphatase inhibitors, and quenching reagents. Cells were lysed by addition of digitonin (1% final concentration) and end-over-end rotation for 1 h at 4 °C. Cell lysates were cleared by centrifugation at 16,000*g* for 10 min at 4 °C and protein concentration was measured using the 660 nm Protein Assay Reagent (Pierce). For each pulldown, 2 mg protein was incubated with Streptavidin Magnetic Beads (Pierce) for 1 h at room temperature with end-over-end rotation. Beads were collected using the DynaMag-2 magnetic stand (Invitrogen) and washed seven times according to the published protocol[35]. Beads were immediately processed for liquid chromatography with MS/MS (LC–MS/MS). Flag immunoprecipitation samples were prepared in the same fashion with the following exceptions: all steps specific to APEX2 proximity labelling were excluded, Anti-Flag M2 Magnetic Beads (Sigma) were used for the pulldown, beads were washed four times with resuspension buffer, and protein was eluted from beads with 3× Flag peptide (Sigma) in resuspension buffer.

On-bead digestion was initiated by addition of 50 μl of 8 M urea in 100 mM Tris to each sample. Samples were reduced and alkylated using 5 mM Tris(2-carboxyethyl)phosphine and 10 mM iodoacetamide, respectively, and digested by addition of lys-C and trypsin proteases at 37 °C while shaking at 800 r.p.m. Digested samples were quenched by addition of formic acid to 5% (v/v) final concentration. Finally, each sample was desalted using C18 tips (87784, Thermo Fisher Scientific) and reconstituted in 5% formic acid before analysis by LC–MS/MS.

Tryptic peptide mixtures were fractionated online using a fused silica with a 75 μm inner diameter and 25 cm long, packed in-house with bulk C18 reversed-phase resin (particle size, 1.9 μm; pore size, 100 Å; Dr. Maisch GmbH). Peptides were separated using a Dionex UltiMate 3000 UHPLC system (Thermo Fisher Scientific). The 140-min water-acetonitrile gradient was delivered at a flow rate of 300 nl min^{-1}. Peptides were ionized, injected into the Orbitrap Fusion Lumos mass spectrometer (Thermo Fisher Scientific) and analysed by MS/MS.

Data were acquired using a Data-Dependent Acquisition method at a MS1 resolution of 120,000, followed by sequential MS2 scans at a resolution of 15,000 to use the remainder of the 3 s cycle time. Data analysis, including peptide and protein identification, was performed using MaxQuant software package v.1.6.3.3 by searching against the mouse UniProt reference proteome (plus the putative sequence for mouse CLSTN3β), followed by filtering of peptide-to-spectrum matches with DTASelect using a spectrum-level false discovery rate of less than 1%.

Proteins identified in the APEX2 samples were filtered for hits that had at least fivefold enrichment over background in both the vehicle and isoproterenol conditions. Background was defined as the sum of two negative controls: (1) brown adipocytes without APEX2 and (2) brown adipocytes with CLSTN3β-APEX2 but without H_2O_2. Intensity was used as a semiquantitative measure of protein abundance. Proteins identified in the Flag immunoprecipitation samples were filtered for hits that were detected in both the vehicle and isoproterenol conditions. High-confidence CLSTN3β binding partners were defined as the intersection between the filtered APEX2 hits and the filtered Flag immunoprecipitation hits. Pathway analysis was carried out using Enrichr[63].

CLSTN3β stability assay

Immortalized brown preadipocytes were differentiated for 6 d and treated with 100 μg ml^{-1} cycloheximide for 0, 2, 4 or 6 h. For each time point, cells were pretreated with either vehicle or 5 μM CB-5083 for 30 min. At the end of the experiment, cells were collected by scraping into PBS, pelleted by centrifugation and lysed by resuspension in YS buffer (50 mM Tris-HCl pH 7.4, 150 mM NaCl, 1% IGEPAL CA-630, protease inhibitors). Lysates were cleared by centrifuging at 12,000*g* for 15 min at 4 °C. Supernatants were retained and protein concentrations

were measured using the 660 nm Protein Assay Reagent (Pierce). Samples were subsequently analysed by western blot. Quantification of band intensities was performed using ImageJ (NIH).

HEK293T cells were cotransfected with CLSTN3β-Flag and either control small-interfering RNA (siRNA) (ON-TARGETplus Non-targeting Control Pool, D-001810-10-05, Horizon) or gp78 siRNA (ON-TARGETplus Human AMFR siRNA SMARTPool, L-006522-00-0005, Horizon) using the TransIT-X2 Dynamic Delivery System (Mirus). Then, 36–48 h after transfection, cells were treated with 100 μg ml^{-1} cycloheximide for 0, 2, 4 or 6 h. At the end of the experiment, cells were collected and analysed as above.

Immunoprecipitation (western blot)

Transfected HEK293T cells were collected by scraping into PBS, pelleted by centrifugation and lysed by resuspension in YS buffer (50 mM Tris-HCl pH 7.4, 150 mM NaCl, 1% IGEPAL CA-630, protease and phosphatase inhibitors). Lysates were cleared by centrifuging at 12,000*g* for 15 min at 4 °C. Supernatants were retained and protein concentrations were measured using the 660 nm Protein Assay Reagent (Pierce). Lysates were incubated with Anti-Flag M2 Magnetic Beads (Sigma) overnight at 4 °C with end-over-end rotation. Beads were collected using the DynaMag-2 magnetic stand (Invitrogen) and washed three times with YS buffer. Protein was eluted from the beads with 3× Flag peptide (Sigma) in YS buffer and samples were analysed by western blot.

Mouse models

CLSTN3β global KO (CLSTN3β KO) mice were generated by the UCSD Transgenic Mouse shared resource on a C57BL/6N background using CRISPR–Cas9 genome editing technology. As outlined in Extended Data Fig. 5a, a single guide RNA was used to introduce random indels at the 3′ end of *Clstn3b* exon 1, creating frameshift mutations in the *Clstn3b* ORF while minimizing disruption of *Clstn3* intron 16. Pups were screened by PCR amplification of genomic DNA followed by Sanger sequencing and CRISP-ID analysis[62], and a single founder with the mutation shown in Extended Data Fig. 5a was selected for colony expansion. Experimental cohorts were generated using a combination of heterozygous (that is, $Clstn3b^{+/-} \times Clstn3b^{+/-}$) and homozygous (that is, $Clstn3b^{+/+} \times Clstn3b^{+/+}$ and $Clstn3b^{-/-} \times Clstn3b^{-/-}$) breeding. Breeders used in homozygous crosses were always derived from heterozygous crosses to minimize genetic drift. Guide RNA and screening or genotyping primers can be found in Supplementary Table 1.

$Clstn3^{f/f}$ mice were generated by Cyagen on a C57BL/6N background with loxP sites flanking exons 17 and 18 (corresponding to exons 2 and 3 of *Clstn3b*), as outlined in Extended Data Fig. 5c. Adipocyte-specific CLSTN3β KO (AdC3KO) mice were generated by crossing $Clstn3^{f/f}$ mice with *Adipoq*-Cre transgenic mice. Experimental cohorts were generated by crossing $Clstn3^{f/f}$;*Adipoq*-Cre^{-} mice with $Clstn3^{f/f}$;*Adipoq*-Cre^{+} mice. Genotyping primers can be found in Supplementary Table 1.

Male *ob/ob* mice on a C57BL/6J background were purchased at 5 weeks of age from The Jackson Laboratory (000632).

Mouse studies

Mouse studies were approved by the Chancellor's Animal Research Committee and were performed in compliance with all relevant ethical regulations. Unless otherwise noted, mice were group housed in a temperature- (roughly 22 °C) and humidity-controlled (on average 50%) facility with a 12-h light and dark cycle and ad libitum access to normal chow diet and water. Experiments were typically performed on age-matched 8–16-week-old littermates. Mice were generally considered to be age matched if their dates of birth were within a 1–2-week period. Mice were typically fasted for 4 h before euthanasia and blood/tissue collection (9:00 to 13:00 local time).

Acute cold challenge. Acute cold challenge was performed by first acclimating mice to thermoneutrality for 2–3 weeks in an environmental chamber set to 30 °C and a 12-h light and dark cycle. Mice were then singly housed at roughly 4 °C in prechilled cages without food or bedding. Core body temperature was monitored hourly for 5–6 h (10:00 to 13:00–14:00 local time) using a BAT-12 Microprobe Thermometer and RET-3 Rectal Probe (Physitemp). Mice were removed from the study and euthanized once their core body temperatures were measured to be 28 °C or lower. If blood or tissues were to be collected and analysed, mice were removed from the study and euthanized at least 1 h before they were expected to reach the 28 °C endpoint.

Cold exposure. Cold exposure was performed by first acclimating mice to single housing for at least 2 d. Mice were then singly housed in an environmental chamber set to 4 °C. Mice had ad libitum access to normal chow diet and water and cages contained bedding and cotton nesting material. Core body temperature was monitored throughout each experiment. Length of cold exposure ranged from 24 h to 8 d.

Rosiglitazone diet. Mice were fed a custom 10% kcal fat diet containing 50 mg kg^{-1} rosiglitazone (Research Diets) for 2 weeks.

HFD. HFD studies were performed on both male and female global and adipocyte-specific CLSTN3β KO mice with both 45 and 60% kcal from fat diets (D12451 and D12492, Research Diets). The 45 and 60% HFD studies were started at 10 and 8 weeks of age, respectively. Body composition was determined by magnetic resonance imaging (EchoMRI) at the beginning and end of each study and body weight was measured weekly. Tissue weights were measured at euthanasia. Glucose tolerance test was performed by fasting HFD-fed mice for 4 h, followed by intraperitoneal injection of 1 mg kg^{-1} glucose and blood glucose measurements at the indicated times.

Metabolic chamber. Respiratory exchange ratios and oxygen consumption (VO_2) were measured by indirect calorimetry using the Oxymax Comprehensive Laboratory Animal Monitoring System (Columbus Instruments). Data were analysed using CalR[64].

^{18}F-FDG PET–CT. Mice were acclimated to single housing overnight. At the start of the following light cycle, mice were housed at 4 °C for 3 h, administered intravenous ^{18}F-FDG through the tail vein and kept at 4 °C for an extra 1 h. PET–CT scans were then performed using the Genisys 8 microPET–CT imaging system (PerkinElmer), and gamma counting on dissected tissues was performed using the 1480 Wizard 3-inch Gamma Counter (PerkinElmer).

AAV. The *Clstn3b* ORF was inserted in reverse orientation in place of enhanced GFP (EGFP) in the AAV8-pCAG-FLEX-EGFP-WPRE vector (Addgene plasmid no. 51502). AAV8-FLEX-EGFP viral particles were purchased from Addgene and AAV8-FLEX-CLSTN3β-Flag viral particles were produced by the University of Michigan Vector Core. Then 10^{12} viral genomes per mouse were injected through the tail vein or subcutaneously in the interscapular region of AdC3KO mice to express GFP or CLSTN3β specifically in adipocytes.

Tissue lipid measurements

BAT was homogenized in JP buffer (10 mM Tris-HCl pH 7.4, 150 mM NaCl, 1 mM EDTA, protease inhibitors) and lipids were extracted from 0.5–1.0 mg of BAT protein using the Bligh and Dyer method. Triglycerides were measured using the Sekisui colorimetric assay.

Histology

Mice were euthanized with isoflurane and blood was extracted by cardiac puncture. Cervical dislocation was performed as a secondary method of euthanasia. BAT, iWAT and/or asWAT were dissected, pieces of tissue were placed in tissue cassettes, and tissue cassettes were

submerged in 10% neutral buffered formalin for 1 week. Cassettes were thoroughly rinsed with running tap water and stored in 70% ethanol. Paraffin embedding, sectioning, haematoxylin and eosin (H&E) staining and anti-CLSTN3 immunohistochemistry (13302-1-AP, Proteintech, 1:100) were done by the UCLA Translational Pathology Core Laboratory. Images were captured using a Zeiss Axioskop 2 Plus equipped with a Zeiss Axiocam 506 Colour.

LD size quantification

For H&E sections, LD size was quantified by measuring the diameter of the ten largest droplets within a representative 100 × 100 μm region from each image. Measurements were recorded in ImageJ (NIH).

For fluorescence microscopy, LD number and size were quantified using a custom CellProfiler (Broad Institute) pipeline. Briefly, individual nuclei were identified using the IdentifyPrimaryObjects module on the DAPI channel. Next, the cell boundaries were estimated using the IdentifySecondaryObjects module by dilating the objects outwards from each nucleus. LDs were identified and characterized using the IdentifySecondaryObjects module on the BODIPY channel, followed by applying the MeasureObjectSizeShape module on the LD objects. Droplets were associated with their respective cells through the RelateObjects module to generate per-cell measurements.

Ex vivo lipolysis assay

iWAT depots were dissected from mice fasted for 3 h. For each replicate, roughly 50 mg tissue from one mouse was minced for 30 s in 400 μl of Krebs–Ringer bicarbonate-modified buffer (135 mM NaCl, 5 mM KCl, 1 mM $MgCl_2$, 1 mM $CaCl_2$, 0.4 mM K_2HPO_4, 25 mM $NaHCO_3$, 10 mM glucose, 20 mM HEPES pH 7.4) with 4% fatty acid-free BSA in a 12-well plate. After mincing, 600 μl of Krebs–Ringer bicarbonate-modified buffer was added to each well and samples were incubated at 37 °C for 3.5 h. Isoproterenol stimulation was performed at a final concentration of 2 μM. After incubation, free fatty acid content in each of the supernatants was quantified using the Wako NEFA kit and values were normalized to tissue weights.

Volumetric imaging of BAT innervation

Visualization of whole BAT sympathetic innervation was achieved using the published Adipo-Clear protocol[65,66] with one critical modification: 3% glyoxal (prepared as described previously[67]) was used in place of 4% paraformaldehyde for fixation because it notably improved visualization of nerve fibre morphology in our side-by-side comparison (Extended Data Fig. 8a). The Adipo-Clear protocol was performed on one random lobe of BAT from each mouse. BAT was treated as a large tissue with respect to incubation times but as a small tissue with respect to incubation volume (that is, 1.6 ml in a 2-ml microcentrifuge tube). Optional steps such as bleaching samples with hydrogen peroxide and embedding samples in agarose were included. Anti-tyrosine hydroxylase antibody (AB1542, Millipore) and donkey anti-sheep IgG Alexa Fluor 568 (A-21099, Thermo Fisher) were used at a 1:200 dilution for immunostaining.

For confocal imaging, samples were mounted in custom chamber slides: 0.5 and 1.0 mm single-sided rectangular iSpacers (SUNJin Lab) were stacked on microscope slides and the chambers were filled with dibenzyl ether and sealed with coverslips (48393-151, VWR) and nail polish. Samples were mounted immediately before imaging and unmounted afterwards to prevent dibenzyl ether from dissolving the chambers.

Samples were imaged using a confocal laser scanning microscope (LSM 880, Zeiss) fitted with a Plan-Apochromat ×10/0.45 M27 objective (2.0 mm working distance). Two images from distinct regions of tissue were acquired for each sample. Each image had an *x* resolution of 0.830 μm, *y* resolution of 0.830 μm and *z* resolution of 11.200 μm. Laser settings were kept constant across all images (except for the *ob/ob* max images, in which laser power was increased to 100%).

Confocal images were analysed on MATLAB (Mathworks) in a blinded fashion. For each image, *z*-stacks were trimmed to eliminate image slices without tissue. Subvolumes of 200 × 200 × 20 voxels were randomly sampled from each trimmed *z*-stack. For each subvolume, tyrosine hydroxylase-positive (TH^+) signal was empirically defined as more than 10% above baseline and less than or equal to 90% of maximum value (to exclude high-intensity signal from vasculature), determined on a slice-by-slice basis. TH^+ signal density was determined for each subvolume. The median TH^+ signal density, calculated from the set of subvolumes, was reported for each sample. A total of 60 subvolumes were analysed for each sample (two *z*-stacks per sample, 30 subvolumes per *z*-stack).

Representative samples were imaged by a blinded experimenter using a light sheet microscope (UltraMicroscope II, LaVision BioTec) equipped with a sCMOS camera (Andor Neo) and a ×2/0.5 numerical aperture objective lens (MVPLAPO ×2) equipped with a 6 mm working distance dipping cap. Samples were scanned with a step size of 3 μm using the continuous light sheet scanning method with the included contrast adaptive algorithm for the 561-nm channel (16 acquisitions per plane). Version 7.1.0 of the ImSpector Pro microscope controller software was used. Three-dimensional reconstructions and animations for Supplementary Videos 1 and 2 were generated using Imaris (Bitplane).

S100B secretion assay

HEK293T cells were seeded on collagen-coated six-well plates overnight and transfected with the indicated constructs using FuGENE 6 transfection reagent (Promega). Then 36–48 h after transfection, cells were gently washed twice with plain DMEM, then incubated with plain DMEM plus vehicle or forskolin (FSK, 5 μM) for the indicated lengths of time. Conditioned media was collected and concentrated using Amicon Ultra-4 centrifugal filters with a 3 kDa cutoff. Conditioned media and whole cell lysates were analysed by western blot.

Seahorse respirometry

Immortalized CLSTN3β KO brown preadipocytes stably expressing mCherry or CLSTN3β-mCherry were differentiated for 4 d in a standard six-well format and then replated in 24-well Seahorse cell culture plates at a density of 20,000 cells per well. On day 6 of differentiation, cells were pretreated with atglistatin (40 μM) or etomoxir (10 μM) for 30–45 min and oxygen consumption rates (OCRs) were measured using a Seahorse XFe24 Analyzer (Agilent). During each run, cells were treated sequentially with isoproterenol (10 μM), oligomycin (oligo, 4 μM), FCCP (2 μM) and rotenone/myxothiazol (7.5 μM). After each run, the total protein content of each well was measured and used to normalize FCCP-induced OCR.

LD isolation

LD isolation was performed on immortalized brown preadipocytes differentiated for 8 d or BAT dissected from mice. Cells were washed twice with PBS, collected by scraping into PBS and pelleted by centrifugation at 1,000*g* for 10 min at 4 °C. Cell pellets were resuspended/tissues were homogenized in Buffer A (20 mM tricine, 250 mM sucrose, pH 7.8, protease inhibitors) and incubated on ice for 20 min. The cell suspension/tissue homogenate was then dounced using the KIMBLE Dounce tissue grinder set (2 ml complete). The lysate was centrifuged at 500*g* for 10 min at 4 °C and large LDs were carefully collected in a minimal volume using a 200 μl pipette tip. The postnuclear supernatant was then transferred to SW 41 Ti tubes, Buffer B (20 mM HEPES, 100 mM KCl, 2 mM $MgCl_2$, pH 7.4) was loaded on top of the postnuclear supernatant, and the gradient was subjected to sequential ultracentrifugation (OptimaTM L-100 XP Ultracentrifuge) at 8,000*g* (medium LDs) and 200,000*g* (small LDs) at 4 °C. After each ultracentrifugation step, LDs were carefully collected in a minimal volume using a 200-μl pipette tip. The 8,000 and 200,000*g* pellets were considered to be mitochondria and ER-enriched membranes and the 200,000*g* supernatant was considered to be cytoplasm. LDs were

washed three times with Buffer B and LD proteins were extracted with 1 ml of acetone for further analysis. LD protein analysis was conducted after normalizing experimental groups on the basis of (1) protein content or (2) triglyceride content. Protein quantification for (1) was estimated by silver stain and triglyceride quantification for (2) was performed using the Folch method of lipid extraction, followed by triglyceride measurement using the Sekisui colorimetric assay.

Human adipose RNAscope

Sections from a human periadrenal adipose tissue microarray were stained using the RNAscope automated chromogenic assay (ACDBio) at the UCLA Translational Pathology Core Laboratory. A custom probe set targeting the unique first exon of human *CLSTN3B* was designed by ACDBio. As described in the original study[48], human periadrenal adipose tissue samples were obtained from control (aldosterone-secreting, cortisol-secreting or non-functioning adrenal tumours) and patients with pheochromocytoma (sporadic, unilateral, benign catecholamine-secreting adrenal tumours) after surgical resection of their tumours. Each patient provided written consent after the study goals, side effects and tissue sampling procedure were explained in detail. The study protocol was reviewed and approved by the UCLA Medical Institutional Review Board. The study was performed in compliance with all relevant ethical regulations.

FRAP-based lipid exchange rate assay

FRAP-based lipid exchange rate assay was performed as described previously[68,69]. Briefly, 3T3-L1 preadipocytes transfected with the indicated plasmids were incubated with 200 μM OA and 1 μg ml^{-1} BODIPY 558/568 C_{12} fatty acid (Molecular Probes) for 16 h and switched to fresh medium 1 h before FRAP experiments. Live cells were visualized under a confocal microscope (A1Rsi, Nikon) using a ×100 oil-immersion objective. LD pairs with clear GFP signal were photobleached. At least 70% of LD total area was photobleached for 1 s at 20% laser power (561-nm solid state laser), followed by time-lapse scanning with a 3 s interval. The same photobleaching process was repeated three times. Mean optical intensities (MOIs) within LD core regions were measured simultaneously. Digital detector gain and laser power were set to avoid overexposure and ensure accurate quantification of fluorescence.

The fluorescence intensities of BODIPY 558/568 C_{12}-labelled triglycerides in the donor (unbleached) and acceptor (bleached) LDs after photobleaching were recorded and normalized by calculating the ratios of their intensities to the initial fluorescence intensity of the acceptor LD at time 0 s after photobleaching. Therefore, the ratio of intensity for the acceptor LD is 1 at the start of the experiment. The normalized ratio of fluorescence intensity of the donor LD at time 0 s after photobleaching is denoted as G_0. Similarly, at any time, the time-dependent normalized ratio of fluorescence intensities of the donor and acceptor LDs are denoted as $G_1(t)$ and $G_2(t)$, respectively. A time-invariable exchange rate ($\emptyset_e$) of neutral lipid molecules between the two LDs can be deduced from the measurement of fluorescence intensities in the LDs with the following equations

$$\emptyset_e = d\ln\left[\frac{G_1(t) - G_2(t)}{1 - G_0}\right]/(-bdt)$$

$$b = \left(\frac{1}{V_1} + \frac{1}{V_2}\right)$$

where V_1 and V_2 represent the volumes of the donor and acceptor LDs, respectively.

Before calculating the lipid exchange rates, the MOIs of both bleached and unbleached LDs were measured with ImageJ (NIH). To obtain fluorescence recovery curves, MOI values were normalized as the percentage of the original fluorescence intensity.

FRAP-based phase separation assay

FRAP-based phase separation assay was performed as described previously[13].

Statistics and reproducibility

Quantitative data presented as bar or line plots show mean ± s.e.m. as well as individual data points where appropriate, with each point representing a biological replicate. Quantitative data presented as violin plots show median (dashed line) and quartiles (dotted lines) as well as the overall data distribution. All statistical tests were two-sided, adjusted for multiple comparisons where appropriate, and performed using GraphPad Prism with standard parameters (assumptions, corrections and so on) after data processing in Microsoft Excel. Exact sample sizes, statistical tests and *P* values can be found in the figure legends and/or source data.

For non-quantitative data (micrographs, western blots and so on), findings were reproduced at least twice by replicating the experiments and/or cross-validating with orthogonal approaches, and representative results are shown.

Reporting summary

Further information on research design is available in the Nature Portfolio Reporting Summary linked to this article.

Data availability

Source data for all figures are provided with the paper. The RNA-sequencing dataset generated for this paper is available at accession number GSE181123. The previously published RNA-sequencing dataset used for LeafCutter splicing analysis in this paper is available at accession number GSE65776. All unique biological materials used are readily available from the authors or from standard commercial sources.

60. Rajbhandari, P. et al. IL-10 signaling remodels adipose chromatin architecture to limit thermogenesis and energy expenditure. *Cell* **172**, 218–233.e17 (2018).
61. Brinkman, E. K., Chen, T., Amendola, M. & Van Steensel, B. Easy quantitative assessment of genome editing by sequence trace decomposition. *Nucleic Acids Res.* **42**, e168–e168 (2014).
62. Dehairs, J., Talebi, A., Cherifi, Y. & Swinnen, J. V. CRISP-ID: decoding CRISPR mediated indels by Sanger sequencing. *Sci. Rep.* **6**, 28973 (2016).
63. Xie, Z. et al. Gene set knowledge discovery with Enrichr. *Curr. Protoc.* **1**, e90 (2021).
64. Mina, A. I. et al. CalR: a web-based analysis tool for indirect calorimetry experiments. *Cell Metab.* **28**, 656–666.e1 (2018).
65. Chi, J. et al. Three-dimensional adipose tissue imaging reveals regional variation in beige fat biogenesis and PRDM16-dependent sympathetic neurite density. *Cell Metab.* **27**, 226–236.e3 (2018).
66. Chi, J., Crane, A., Wu, Z. & Cohen, P. Adipo-clear: a tissue clearing method for three-dimensional imaging of adipose tissue. *J. Vis. Exp.* **2018**, 58271 (2018).
67. Richter, K. N. et al. Glyoxal as an alternative fixative to formaldehyde in immunostaining and super-resolution microscopy. *EMBO J.* **37**, 139–159 (2018).
68. Wang, J. et al. Polybasic RKKR motif in the linker region of lipid droplet (LD)–associated protein CIDEC inhibits LD fusion activity by interacting with acidic phospholipids. *J. Biol. Chem.* **293**, 19330–19343 (2018).
69. Wang, J., Chua, B. T., Li, P. & Chen, F.-J. Lipid-exchange rate assay for lipid droplet fusion in live cells. *Bio-Protocol* **9**, e3309 (2019).

Acknowledgements We thank H. Yang for sharing valuable expertise. We thank A. Ferrari, J. Sandhu, P. Rajbhandari and all other current and former members of the Tontonoz laboratory for technical assistance and valuable discussions. We thank S. Zhang for unwavering support. Confocal microscopy was performed at the California NanoSystems Institute Advanced Light Microscopy and Spectroscopy Laboratory. PET–CT was performed at the Crump Institute Preclinical Imaging Technology Center. RNAscope was performed at the UCLA Translational Pathology Core Laboratory. This work was supported by grants from the the National Natural Science Foundation of China (grant no. 91857103 to F.-J.C.), NIH (grant nos. R01DK120851 and R01HL136618 to P.T.) and Fondation Leducq (grant no. 19CVD04 to P.T.). K.Q. was supported by grant no. NIH F30DK123986 and a David Geffen Medical Scholarship.

Author contributions Conceptualization was done by K.Q., M.J.T., P.L. and P.T. Methodology was developed by K.Q., M.J.T., L.C., A.H.B., T.A.W., P.S.R., Y.S., B.T.B., J.P.W., J.A.W. and P.L. Software was written by K.Q., B.T.B. and C.-H.L. Validation was carried out by K.Q., M.J.T., J.W., L.F.U., X.X., L.C., A.H.B., T.A.W., P.S.R., L.V., Y.S., Y.Y., Y.J.-A., W.C. and B.J. Formal analysis was carried out by K.Q., M.J.T., J.W., A.H.B., L.V., Y.J.-A., W.C., B.T.B. and C.-H.L. Investigation was

done by K.Q., M.J.T., J.W., L.F.U., X.X., L.C., A.H.B., T.A.W., P.S.R., L.V., Y.S., Y.Y., Y.J.-A., W.C. and B.J. Resources were provided by L.A.D., D.L.B., J.P.W., J.A.W., K.R., K.S., F.-J.C., S.G.Y., P.L. and P.T. Data were curated by K.Q., M.J.T., J.W., L.F.U., A.H.B., T.A.W., P.S.R., L.V., Y.Y., Y.J.-A., W.C., B.T.B., C.-H.L. and B.J. The original draft was written by K.Q. and P.T. Review and editing of the draft were done by K.Q., M.J.T., J.W., L.F.U., X.X., L.C., A.H.B., T.A.W., P.S.R., L.V., Y.S., Y.Y., Y.J.-A., W.C., B.T.B., C.-H.L., B.J., L.A.D., D.L.B., J.P.W., J.A.W., K.R., K.S., F.-J.C., S.G.Y., P.L. and P.T. Visualization was done by K.Q., M.J.T., J.W., L.F.U., X.X., L.C., A.H.B., T.A.W., P.S.R., Y.Y., C.-H.L., B.J. and P.T. Supervision was the responsibility of K.Q., D.L.B., K.R., F.-J.C., S.G.Y., P.L. and P.T. Project administration was done by K.Q., F.-J.C., P.L. and P.T. Funding was acquired by S.G.Y., P.L. and P.T.

Competing interests The authors declare no competing interests.

Additional information

Supplementary information The online version contains supplementary material available at https://doi.org/10.1038/s41586-022-05507-1.

Correspondence and requests for materials should be addressed to Peter Tontonoz.

Peer review information *Nature* thanks the anonymous reviewers for their contribution to the peer review of this work.

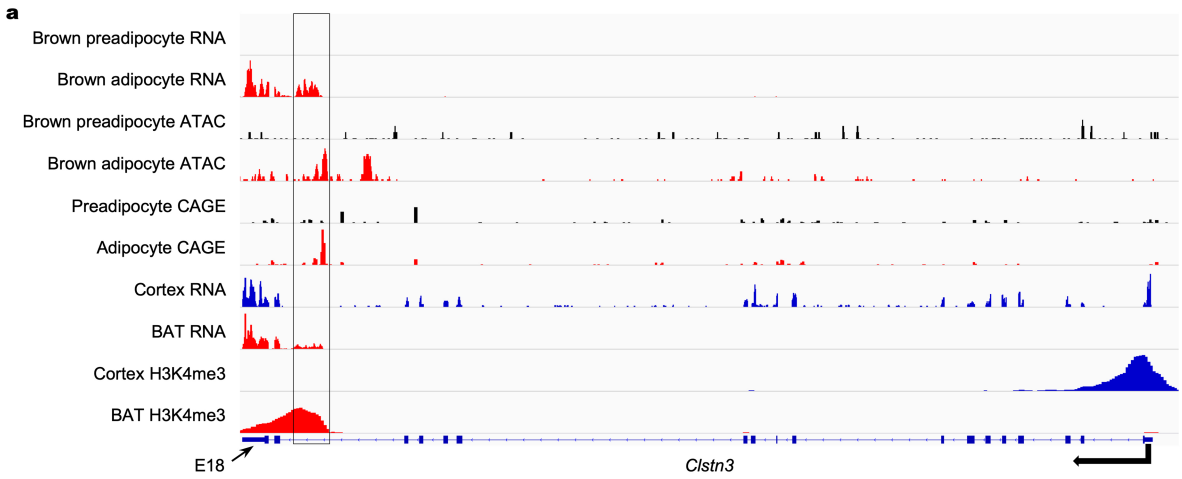

b

Transcript variant	Abundance
1	55%
2	30% (+ 5.3%*)
3	9.3%
4	?

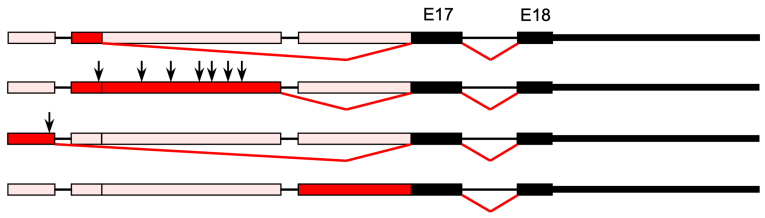

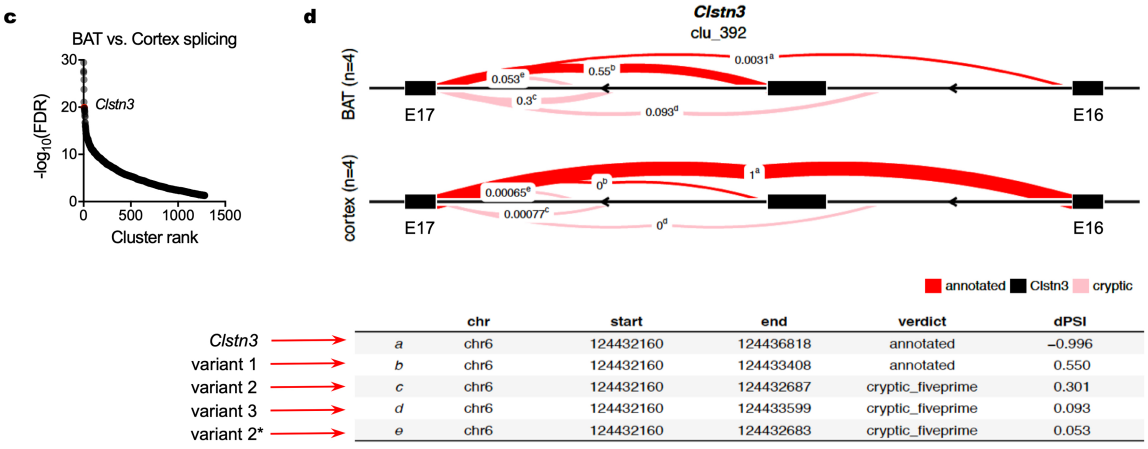

		chr	start	end	verdict	dPSI
Clstn3	a	chr6	124432160	124436818	annotated	−0.996
variant 1	b	chr6	124432160	124433408	annotated	0.550
variant 2	c	chr6	124432160	124432687	cryptic_fiveprime	0.301
variant 3	d	chr6	124432160	124433599	cryptic_fiveprime	0.093
variant 2*	e	chr6	124432160	124432683	cryptic_fiveprime	0.053

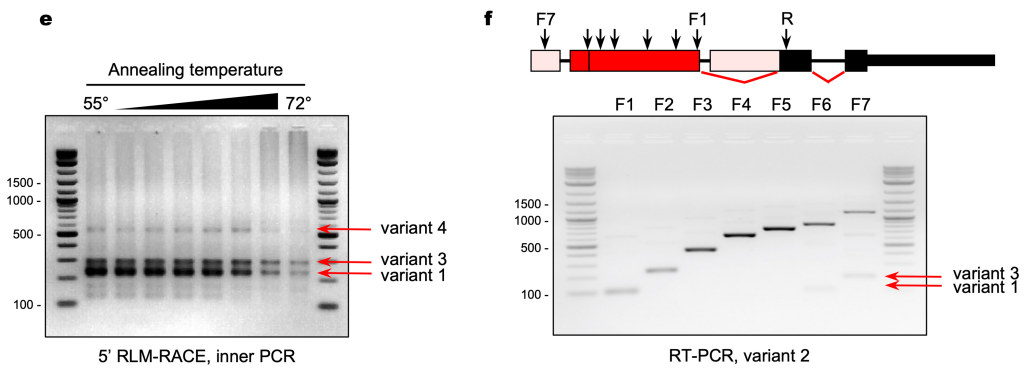

Extended Data Fig. 1 | Identification of *Clstn3b* transcript species. **a**, RNA-, ATAC-, CAGE-, and H3K4me3 ChIP-seq reads at the *Clstn3* locus in mouse preadipocytes (day 0 of differentiation), adipocytes (day 5 of differentiation), cortex, and BAT. **b**, Summary of mouse *Clstn3b* transcript variants. Arrows mark positions of possible start codons (ATGs that are in-frame with *Clstn3* exons 17/18). **c**, LeafCutter analysis of differential splice site utilization in mouse BAT and cerebral cortex. Intron clusters are ranked by statistical significance. *Clstn3* (rank 8) is highlighted in red. **d**, LeafCutter output for the *Clstn3* intron cluster. **e**, 5′RLM-RACE products from mouse BAT using gene-specific primers targeting *Clstn3* exon 17. **f**, RT-PCR products from mouse BAT using primers targeting *Clstn3b* transcript variant 2. Black arrows mark positions of primers (F1-F7 = forward 1 through forward 7, R = reverse). *This splice site is actually two splice sites that are 4 base pairs apart. One (30%) is in-frame with *Clstn3* exons 17/18 and produces a protein-coding transcript. The other (5.3%) is out-of-frame with *Clstn3* exons 17/18 and produces a non-coding transcript.

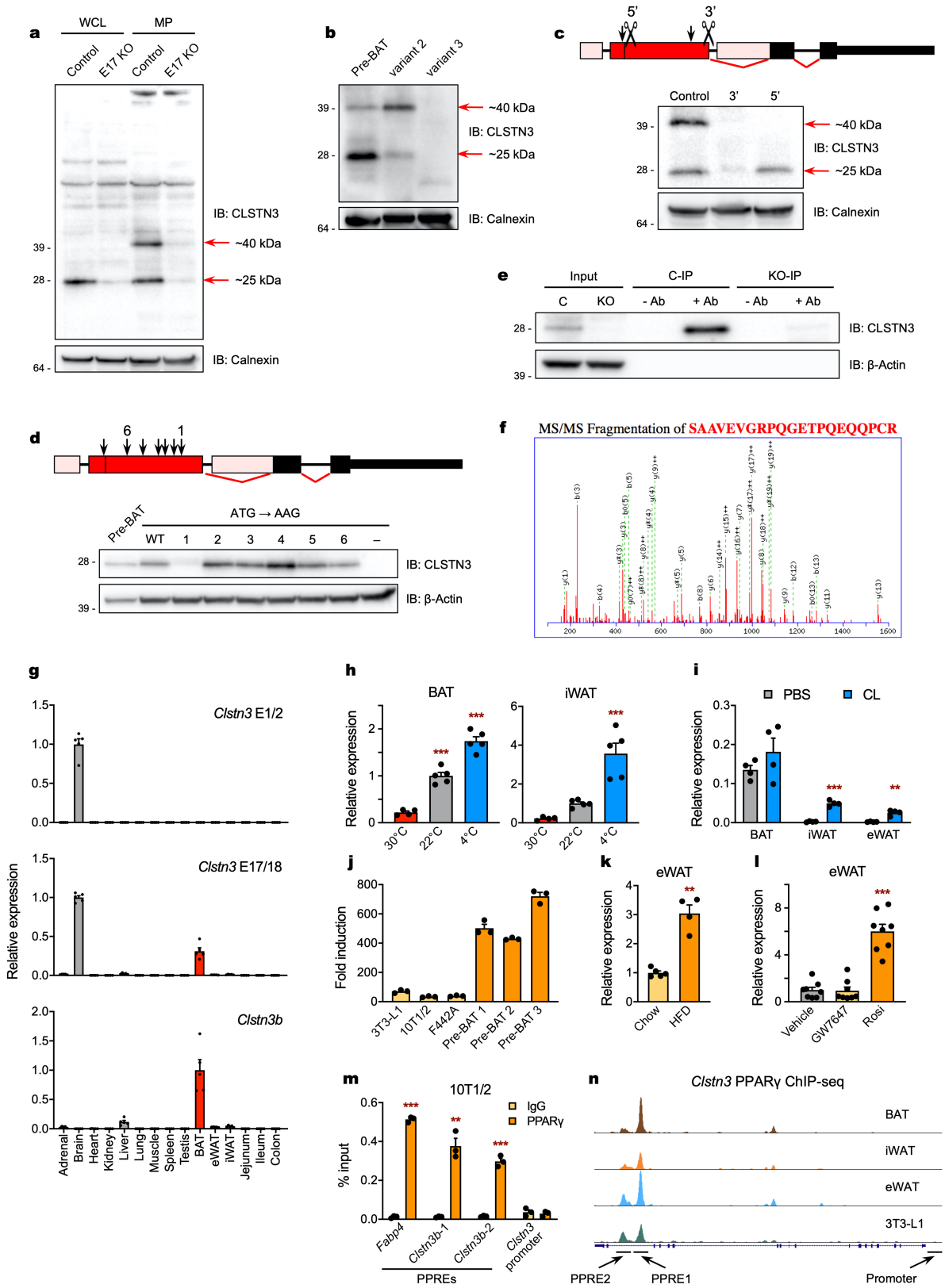

Extended Data Fig. 2 | See next page for caption.

Extended Data Fig. 2 | Identification of CLSTN3β protein species and transcriptional regulation of *Clstn3b*. **a**, Whole cell lysates (WCL) and membrane preparations (MP) of control and *Clstn3* exon 17 KO Pre-BAT cells (pools of CRISPR-modified immortalized brown preadipocytes differentiated for 5 days). Western blot analysis with a previously unvalidated commercial antibody targeting the C-terminus of CLSTN3 (shared with CLSTN3β) identifies two specific bands in brown adipocytes. **b**, Membrane preparations of Pre-BAT cells (day 5 of differentiation) and HeLa cells transfected with *Clstn3b* transcript variant 2 or 3 (only variants with protein-coding potential). Western blot analysis with the CLSTN3 antibody shows that *Clstn3b* transcript variant 2 produces two bands of the same size as those expressed endogenously in brown adipocytes. **c**, Membrane preparations of three different Pre-BAT CRISPR pools: control, 3′ (gRNA targeting 3′ end of variant 2, downstream of all possible start codons), and 5′ (gRNA targeting 5′ end of variant 2, downstream of start codon generating longest ORF). Scissors mark positions of gRNAs and black arrows mark possible start codons immediately upstream of gRNAs. Western blot analysis with the CLSTN3 antibody shows that the ~25 kDa band is not a cleavage product of the ~40 kDa band and can be translated from variant 2 independently. **d**, Whole cell lysates of Pre-BAT cells (day 5 of differentiation) and HeLa cells transfected with *Clstn3b* transcript variant 2 containing ATG to AAG mutations at each possible start codon (positions marked by arrows). Western blot analysis with the CLSTN3 antibody shows that the first possible start codon (generating shortest ORF) initiates translation of a ~25 kDa protein product. **e**, Immunoprecipitation (IP) of the endogenous ~25 kDa protein from control (C) and 3′ gRNA (KO) Pre-BAT CRISPR pools (day 5 of differentiation) using the CLSTN3 antibody. **f**, Fragmentation spectrum of a CLSTN3β-specific peptide identified by IP-MS/MS. **g**, qPCR analysis of *Clstn3* exons 1/2, *Clstn3* exons 17/18, and *Clstn3b* expression in a panel of 15 mouse tissues ($n = 5$). **h**, (Left) *Clstn3b* expression in BAT of mice housed at 30 °C for 2 weeks, 22 °C, or 4 °C for 24 h ($n = 4, 5, 5$). (Right) *Clstn3b* expression in iWAT of mice housed at 30 °C for 2 weeks, 22 °C, or 4 °C for 48 h ($n = 4, 5, 5$). **i**, *Clstn3b* expression in BAT, iWAT, and eWAT of mice injected with PBS or 1 mg/kg/day CL-316,243 (CL) for 4 days ($n = 4$). **j**, Fold induction of *Clstn3* exons 17/18 expression from day 0 to day 5 of differentiation in white and brown preadipocyte cell lines ($n = 3$). 3T3-L1, (C3H/)10T1/2, and (3T3-)F442A refer to three commonly-used white preadipocyte cell lines. Pre-BAT 1, 2, and 3 refer to three distinct single cell clones isolated from a pool of immortalized primary mouse brown preadipocytes. **k**, *Clstn3b* expression in eWAT of mice fed normal chow or a 60% high-fat diet (HFD) for 4 days ($n = 5, 4$). **l**, *Clstn3b* expression in eWAT of mice gavaged with vehicle, GW7647 (PPARα agonist, 10 mg/kg), or rosiglitazone (PPARγ agonist, 10 mg/kg) 3 times in 2 days ($n = 8$). **m**, ChIP-qPCR analysis of PPARγ binding to *Fabp4*, *Clstn3b*, and *Clstn3* promoter elements in 10T1/2 cells ($n = 3$). **n**, PPARγ ChIP-seq reads at the *Clstn3* locus in primary mouse BAT, iWAT, and eWAT adipocytes and 3T3-L1 cells. Genomic regions targeted in ChIP-qPCR experiment (**m**) are annotated. Bar plots show mean ± SEM. Each point represents a biological replicate. Two-sided $^{**}P < 0.01$, $^{***}P < 0.001$ by ordinary one-way ANOVA with Dunnett's multiple comparisons test (**h**, **l**), multiple t-tests with Holm-Sidak correction (**i**, **m**), or Welch's t-test (**k**).

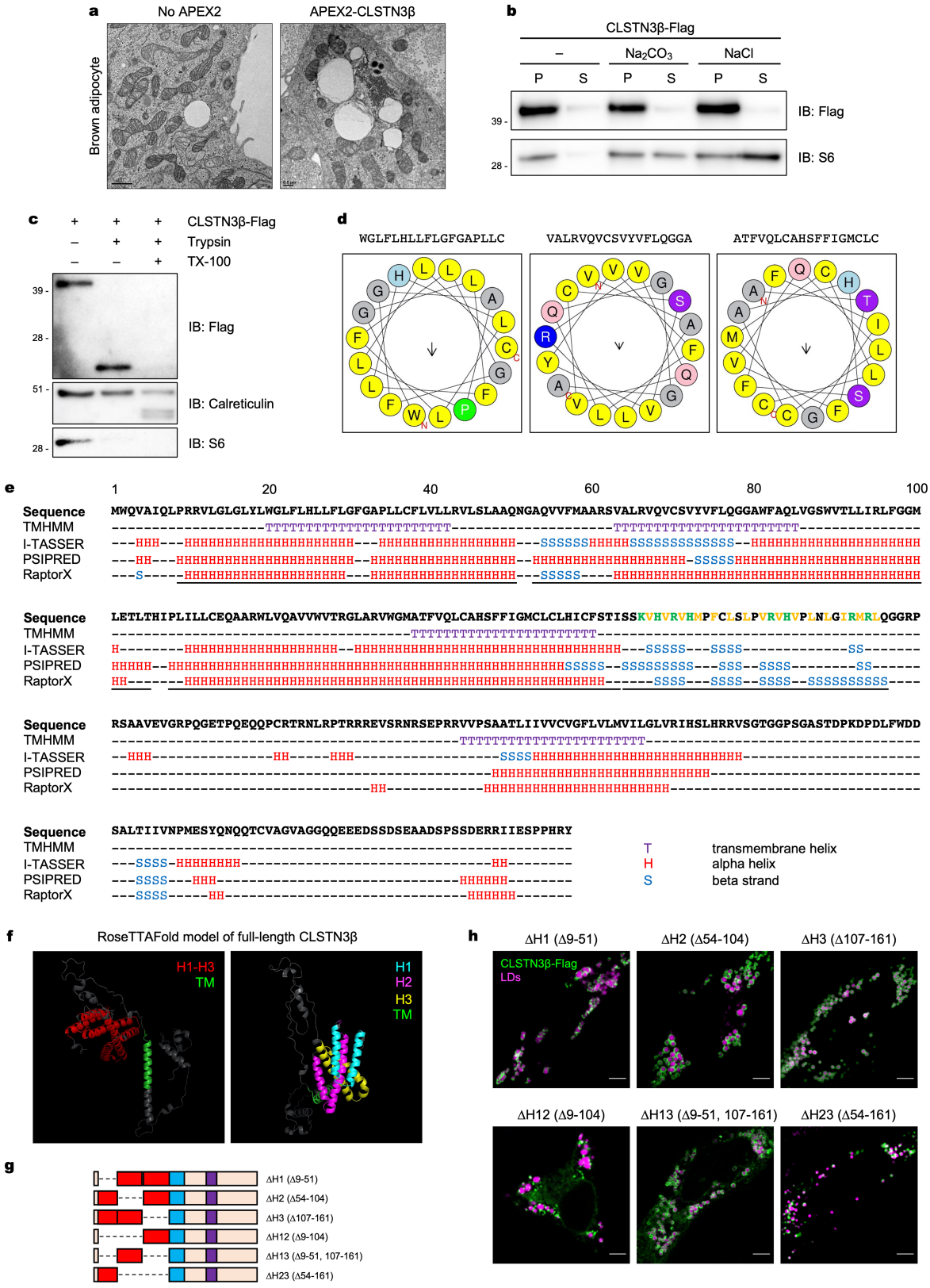

Extended Data Fig. 3 | See next page for caption.

Extended Data Fig. 3 | Structural features of CLSTN3β. a, Electron microscopy of immortalized brown adipocytes (day 4 of differentiation) stably expressing (left) no APEX2 or (right) an N-terminal APEX2-CLSTN3β fusion. APEX2-CLSTN3β is poorly expressed and thus its localization is not visualized. **b**, Biochemical extraction of CLSTN3β-Flag (integral membrane protein) and S6 (peripheral membrane protein) from membranes of HEK293T cells treated with OA (250 μM, overnight). P = pellet, S = supernatant. **c**, Protease protection assay on membranes from HEK293T cells transfected with CLSTN3β-Flag (C-terminal tag) and treated with OA (250 μM, overnight). Calreticulin = inside ER, S6 = outside ER. **d**, Helical wheel plots of representative α-helices from CLSTN3β, generated using HeliQuest. **e**, Summary of CLSTN3β secondary structure predictions. Putative hydrophobic hairpins and β-strand domain are underlined. Positively charged and hydrophobic residues in the β-strand domain are colored green and yellow, respectively. **f**, RoseTTAFold model of full-length CLSTN3β. (Left) Model positioned to highlight hairpin domain (red) and TM domain (green). (Right) Model positioned to highlight hairpin 1 (cyan), hairpin 2 (magenta), hairpin 3 (yellow), and TM domain (green). **g**, Schematic of CLSTN3β hairpin mutants. **h**, Confocal microscopy of OA-treated (1 mM, overnight) HeLa cells transfected with ΔH1, ΔH2, ΔH3, ΔH12, ΔH13, or ΔH23 CLSTN3β-Flag constructs and stained with BODIPY 488 or LipidTOX 647. Scale bar = 5 μm.

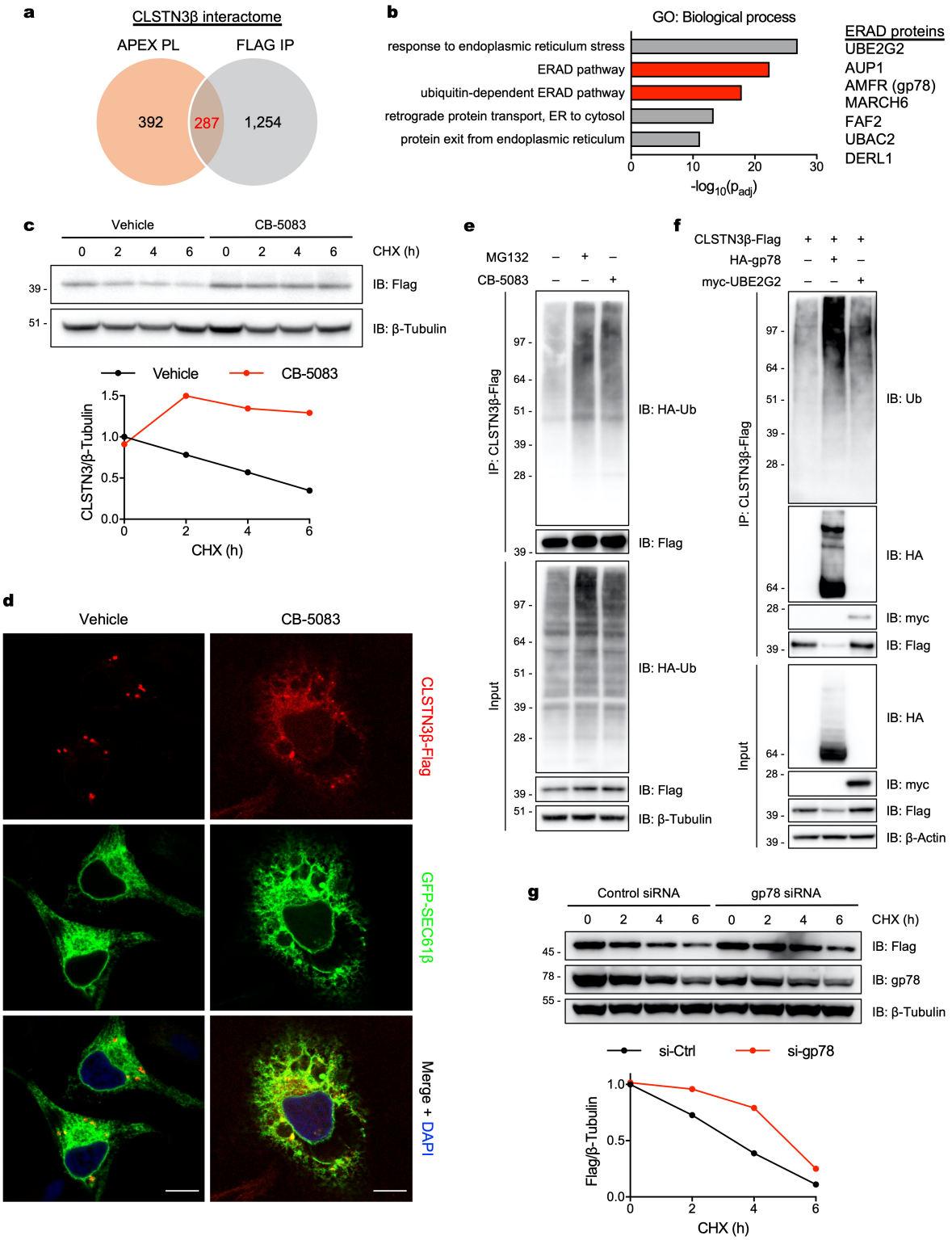

Extended Data Fig. 4 | ER-localized CLSTN3β is degraded by ERAD. a, Venn diagram showing the number of proteins identified as potential CLSTN3β binding partners by APEX proximity labeling (PL) and Flag immunoprecipitation (IP). **b**, (Left) Gene ontology (GO) analysis of the high-confidence CLSTN3β interactome (287 proteins). (Right) Partial list of ERAD proteins in the high-confidence CLSTN3β interactome. **c**, Immortalized brown adipocytes (day 6 of differentiation) were treated with cycloheximide (CHX, 100 μg/mL) for the indicated times and pretreated with either vehicle (DMSO) or CB-5083 (5 μM) for 30 min. **d**, Confocal microscopy of HeLa cells transfected with CLSTN3β-Flag and GFP-SEC61β and treated with either vehicle (DMSO) or CB-5083 (2.5 μM) for 8 h. Scale bar = 10 μm. **e**, CLSTN3β-Flag immunoprecipitation from HEK293T cells co-transfected with HA-ubiquitin and treated with either MG132 (25 μM) or CB-5083 (2.5 μM) for 4 h. **f**, CLSTN3β-Flag immunoprecipitation from HEK293T cells co-transfected with either HA-gp78 or myc-UBE2G2 and treated with CB-5083 (2.5 μM) for 4 h. **g**, HEK293T cells were co-transfected with CLSTN3β-Flag and either control or gp78 siRNA and treated with CHX (100 μg/mL) for the indicated times.

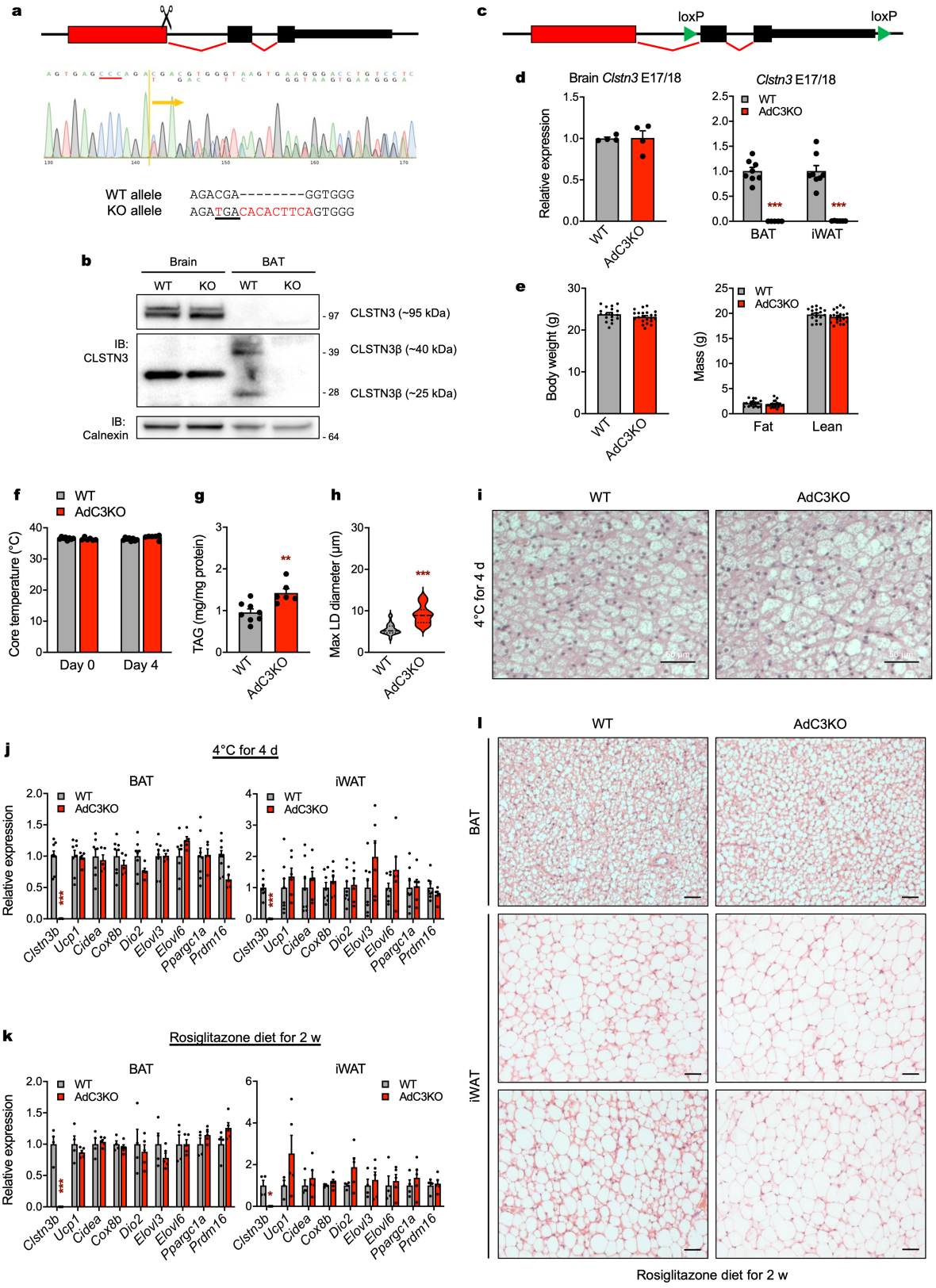

Extended Data Fig. 5 | See next page for caption.

Extended Data Fig. 5 | Analysis of thermogenesis in CLSTN3β-deficient mice. a, (Top) Schematic of CRISPR strategy used to generate CLSTN3β KO mice. Scissors mark position of gRNA. (Middle) CRISP-ID analysis of Sanger sequencing trace from CLSTN3β KO founder. PAM sequence is underlined in red. (Bottom) Nucleotide sequences of WT and CLSTN3β KO alleles. Bases altered in KO allele are highlighted in red and premature stop codon is underlined. **b**, Western blot analysis of membrane preparations of brain and BAT from WT and CLSTN3β KO mice housed at 22 °C. **c**, Schematic of Cre-Lox strategy used to generate AdC3KO mice. **d**, qPCR analysis of *Clstn3* exons 17/18 expression in (left) brain from WT and AdC3KO mice housed at 22 °C ($n = 4, 4$) and (right) BAT and iWAT from WT and AdC3KO mice housed at 4 °C for 4 days ($n = 8, 6$). **e**, Body weights and compositions of 10-12 week-old male WT and AdC3KO mice on a normal chow diet ($n = 18, 22$). **f**, Core body temperatures, **g**, BAT TAG content, and **h**, diameters of largest LDs ($n = 40, 40$) in **i**, H&E sections of BAT from 10-11 week-old male WT and AdC3KO mice housed at 4 °C for 4 days ($n = 8, 6$). Scale bar = 50 µm. **j**, qPCR analysis of BAT and iWAT from 10-11 week-old male WT and AdC3KO mice housed at 4 °C for 4 days ($n = 8, 6$). **k**, qPCR analysis and **l**, H&E sections of BAT and iWAT from 12-14 week-old male WT and AdC3KO mice fed a 10% kcal fat diet containing 50 mg/kg rosiglitazone for 2 weeks ($n = 4, 5$). Scale bar = 50 µm. Bar plots show mean ± SEM. Each point represents a biological replicate. Violin plots show median (dashed) and quartiles (dotted). Two-sided $^{*}P < 0.05$, $^{**}P < 0.01$, $^{***}P < 0.001$ by multiple t-tests with Holm-Sidak correction (**d**, **j**-**k**) or Welch's t-test (**g**-**h**).

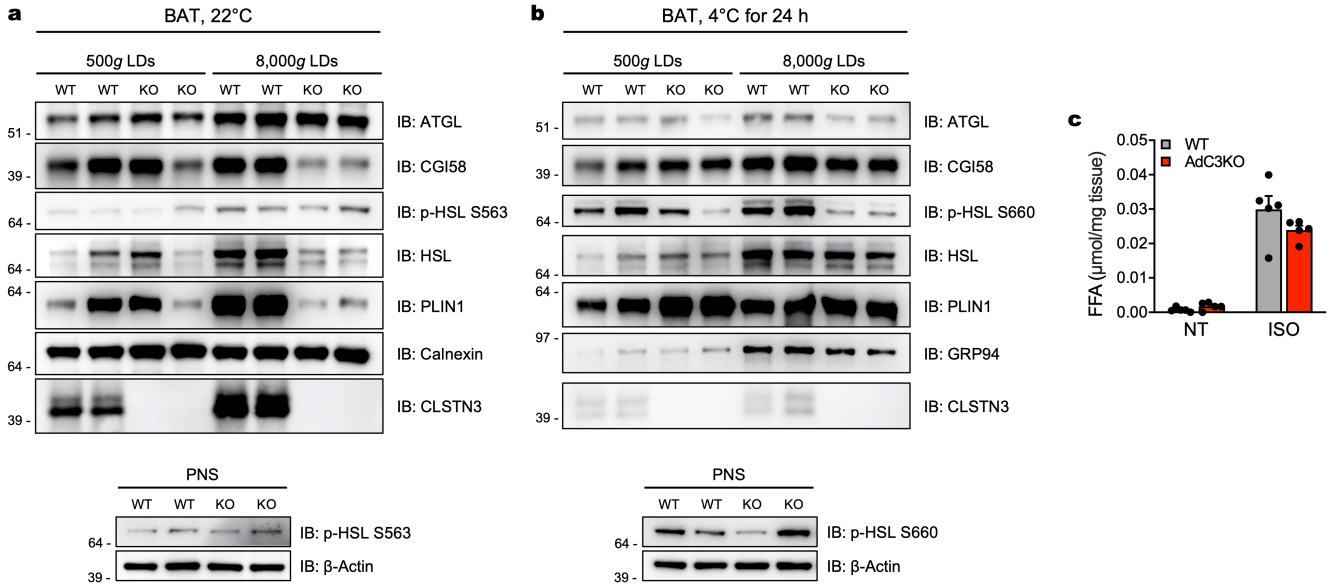

Extended Data Fig. 6 | Analysis of lipolysis in CLSTN3β-deficient mice. (**a-b**), Western blot analysis of BAT LDs and post-nuclear supernatants (PNS) isolated from female WT and AdC3KO mice housed at 22 °C or 4 °C for 24 h (n = 2 mice per lane). Equal amounts of TAG from each condition were loaded onto the gels. From the same experiment as Fig. 5l. **c**, *Ex vivo* lipolysis assay performed on iWAT from 11-12 week-old female WT and AdC3KO mice (n = 5, 5). NT = no treatment, ISO = isoproterenol (2 µM). Bar plots show mean ± SEM. Each point represents a biological replicate.

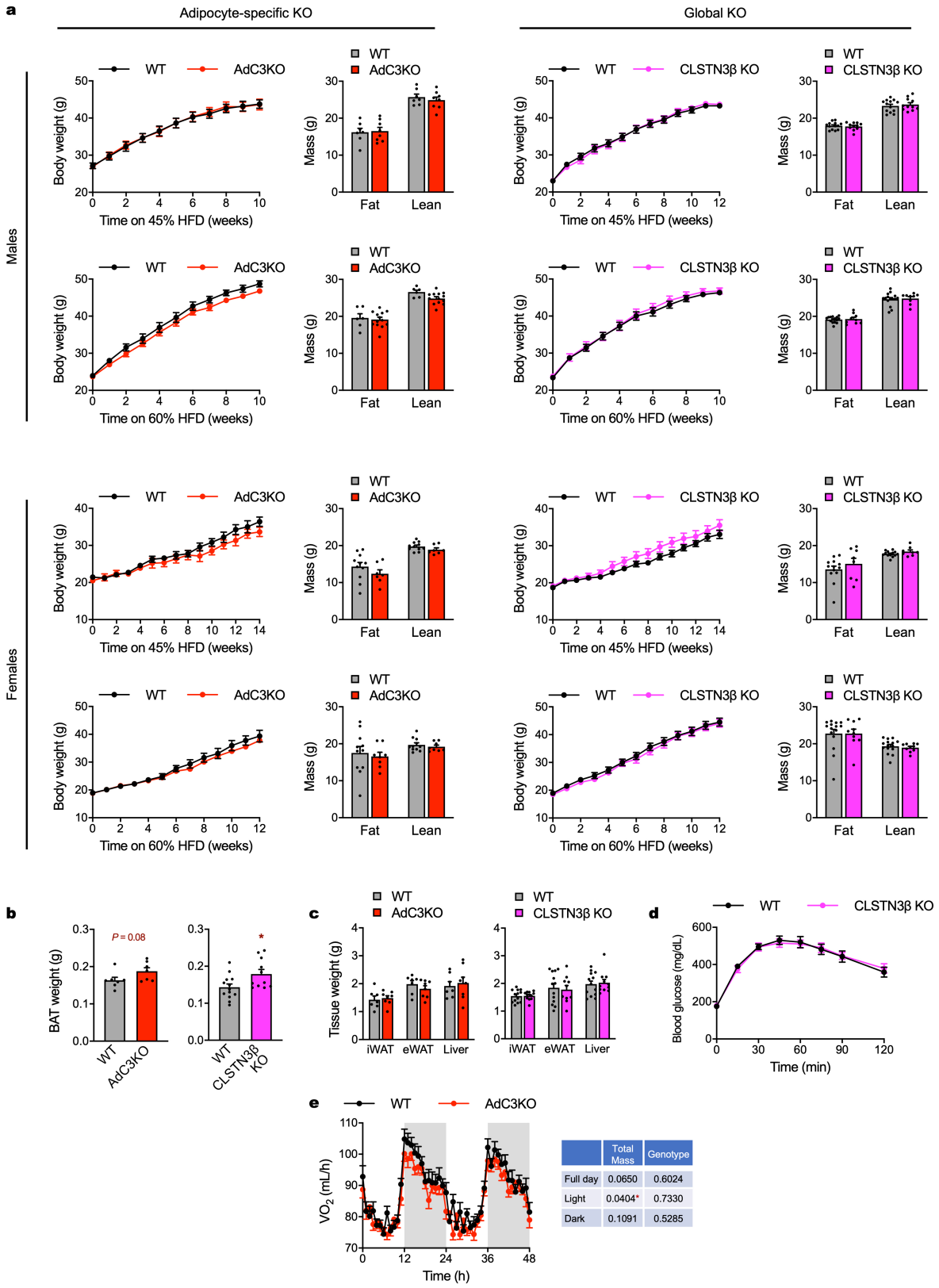

Extended Data Fig. 7 | See next page for caption.

Extended Data Fig. 7 | Characterization of CLSTN3β-deficient mice on a HFD. a, Body weights and compositions of male and female WT/AdC3KO and WT/CLSTN3β KO mice on 45% and 60% HFD. Male WT/AdC3KO 45% HFD ($n = 7, 8$), male WT/AdC3KO 60% HFD ($n = 6, 13$), female WT/AdC3KO 45% HFD ($n = 11, 7$), female WT/AdC3KO 60% HFD ($n = 11, 8$), male WT/CLSTN3β KO 45% HFD ($n = 13, 11$), male WT/CLSTN3β KO 60% HFD ($n = 15, 9$), female WT/CLSTN3β KO 45% HFD ($n = 13, 8$), female WT/CLSTN3β KO 60% HFD ($n = 15, 10$). **b**, BAT weights from (left) male WT and AdC3KO mice on a 45% HFD for 10 weeks ($n = 7, 7$) or (right) male WT and CLSTN3β KO mice on a 45% HFD for 12 weeks ($n = 13, 11$). **c**, iWAT, eWAT, and liver weights from (left) male WT and AdC3KO mice on a 45% HFD for 10 weeks ($n = 7, 8$) or (right) male WT and CLSTN3β KO mice on a 45% HFD for 12 weeks ($n = 13, 11$). **d**, Intraperitoneal glucose tolerance test performed on male WT and CLSTN3β KO mice on a 45% HFD for 12 weeks ($n = 6, 6$). **e**, Oxygen consumption (VO_2) in 10-12 week-old male WT and AdC3KO mice housed at 22 °C and fed a normal chow diet ($n = 18, 22$). Bar/line plots show mean ± SEM. Each point represents a biological replicate. Two-sided $^*P < 0.05$ by Welch's t-test (**b**) or ANOVA (**e**).

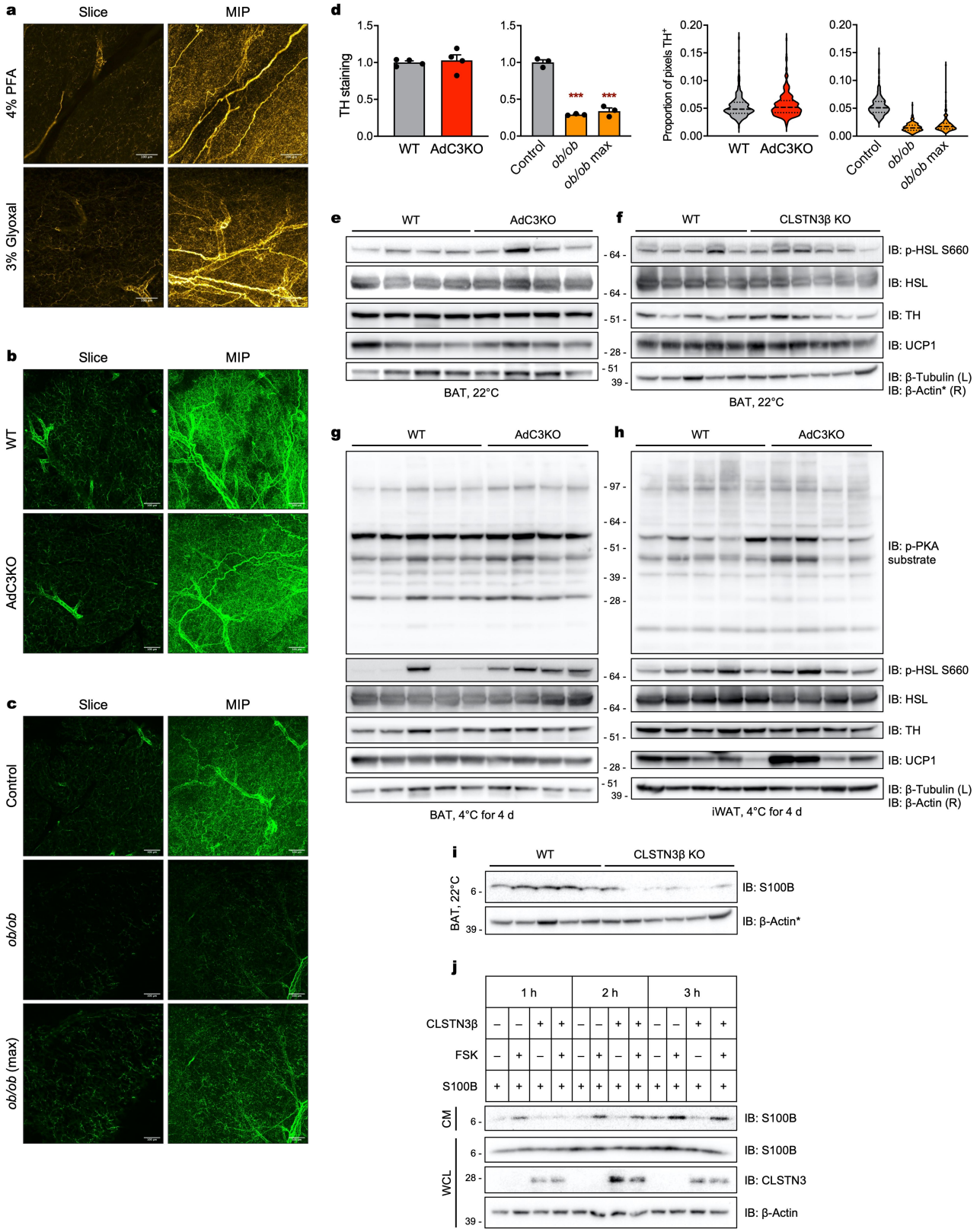

Extended Data Fig. 8 | See next page for caption.

Extended Data Fig. 8 | Analysis of adipose innervation and adrenergic signaling in CLSTN3β-deficient mice. (**a**–**c**) Representative slices and maximum intensity projections (MIPs) of whole BAT lobe tyrosine hydroxylase (TH) immunostaining. Scale bar = 100 μm. **a**, 4% paraformaldehyde (PFA) vs. 3% glyoxal fixation. **b**, 11-12 week-old male WT and AdC3KO mice housed at 22 °C. **c**, 5–6 week-old male control and *ob/ob* mice housed at 22 °C. *ob/ob* samples were imaged at the same laser power as control samples as well as at maximum laser power. Control vs. *ob/ob* comparison was performed as a positive control for differences in BAT TH immunostaining. **d**, Quantification of TH staining in WT vs. AdC3KO ($n = 4, 4$) and control vs. *ob/ob* ($n = 3, 3$) mice. (Left) One value reported per mouse, (right) one value reported per sub-volume (60 sub-volumes per mouse). Western blot analysis of **e**, BAT from 11 week-old male WT and AdC3KO mice housed at 22 °C, **f**, BAT from 17-18 week-old male WT and CLSTN3β KO mice housed at 22 °C, **g**, BAT from 10-11 week-old male WT and AdC3KO mice housed at 4 °C for 4 days, **h**, iWAT from 10-11 week-old male WT and AdC3KO mice housed at 4 °C for 4 days, and **i**, BAT from 17-18 week-old male WT and CLSTN3β KO mice housed at 22 °C. **j**, Western blot analysis of conditioned media (CM) and whole cell lysates (WCL) from HEK293T cells transfected/treated with the indicated constructs/compounds. FSK = forskolin (5 μM). *These β-Actin blots are the same. Extended Data Fig. 8F, I are from the same experiment but were split up for presentation purposes. Bar plots show mean ± SEM. Each point represents a biological replicate. Violin plots show median (dashed) and quartiles (dotted). Two-sided $^{***}P < 0.001$ by ordinary one-way ANOVA with Dunnett's multiple comparisons test (**d**).

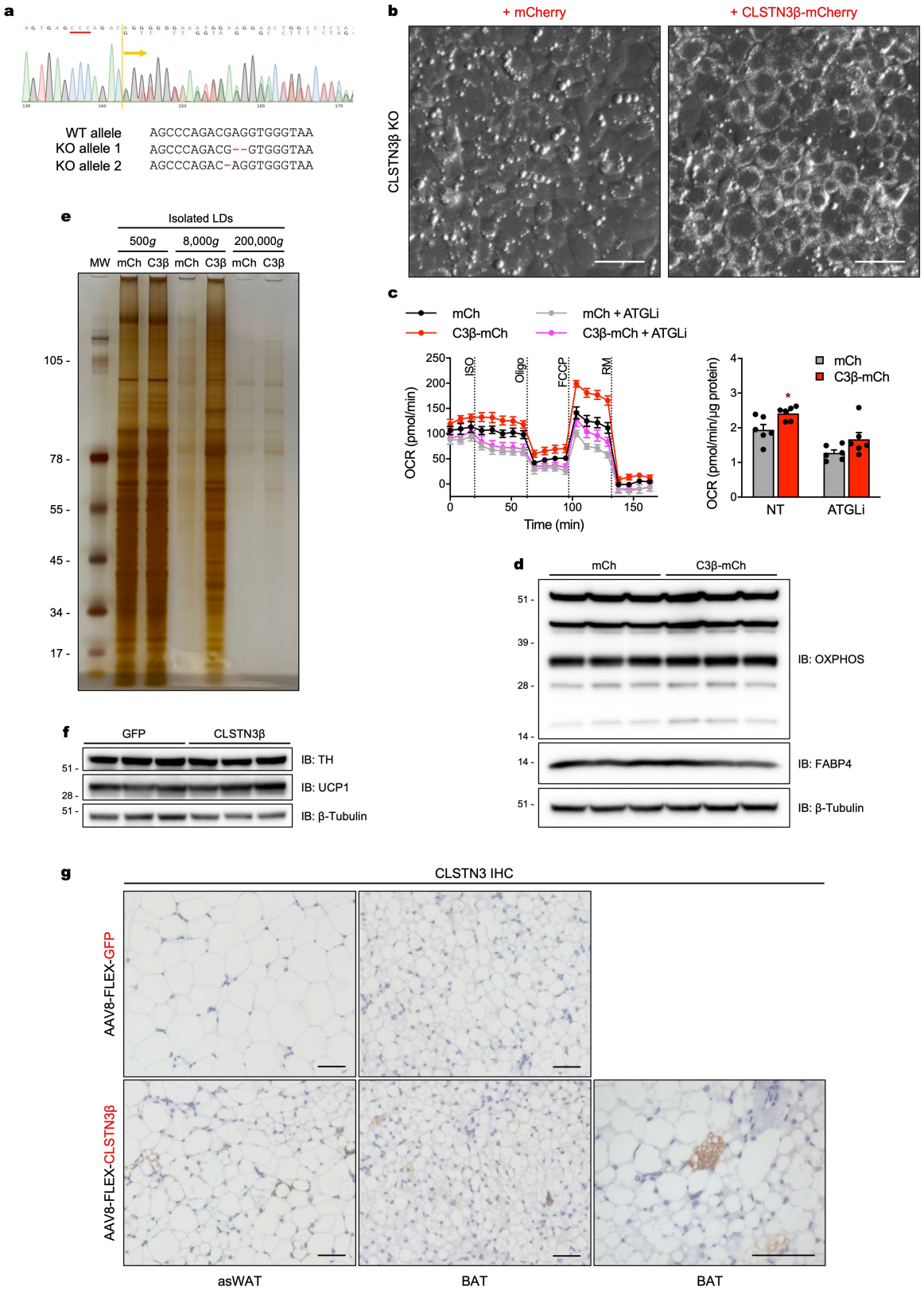

Extended Data Fig. 9 | See next page for caption.

Extended Data Fig. 9 | Characterization of cells and mice re-expressing CLSTN3β. a, (Top) CRISP-ID analysis of Sanger sequencing trace from immortalized CLSTN3β KO brown preadipocyte clone. PAM sequence is underlined in red. CRISPR strategy is identical to that depicted in Extended Data Fig. 5A. (Bottom) Nucleotide sequences of WT and CLSTN3β KO alleles. Bases deleted in KO alleles are highlighted in red. **b**, Light microscopy of immortalized CLSTN3β KO brown adipocytes stably expressing (left) mCherry or (right) CLSTN3β-mCherry (day 5 of differentiation). Scale bar = 50 μm. **c**, (Left) Seahorse respirometry analysis of oxygen consumption rates (OCR) in immortalized CLSTN3β KO brown adipocytes stably expressing mCherry (mCh) or CLSTN3β-mCherry (C3β-mCh) (day 6 of differentiation) and treated with isoproterenol (ISO, 10 μM), oligomycin (oligo, 4 μM), FCCP (2 μM), and rotenone/myxothiazol (RM, 7.5 μM). Cells were pre-treated with atglistatin (ATGLi, 40 μM) for 30-45 min where indicated. (Right) FCCP-induced OCR normalized to protein content ($n = 6$). **d**, Western blot analysis of immortalized CLSTN3β KO brown adipocytes stably expressing mCh or C3β-mCh (day 6 of differentiation). **e**, Silver stain analysis of large (500 *g*), medium (8,000 *g*), and small (200,000 *g*) LDs isolated from immortalized CLSTN3β KO brown adipocytes stably expressing mCh or C3β-mCh (day 8 of differentiation). Equal amounts of TAG from each condition were loaded onto the gel. **f**, Same experiment as Fig. 4A–E. Western blot analysis of BAT. **g**, Same experiment as Fig. 4F. CLSTN3 immunohistochemistry (IHC) of asWAT and BAT. Scale bar = 50 μm. Bar/line plots show mean ± SEM. Each point represents a biological replicate. Two-sided $^*P < 0.05$ by multiple t-tests with Holm-Sidak correction (**c**).

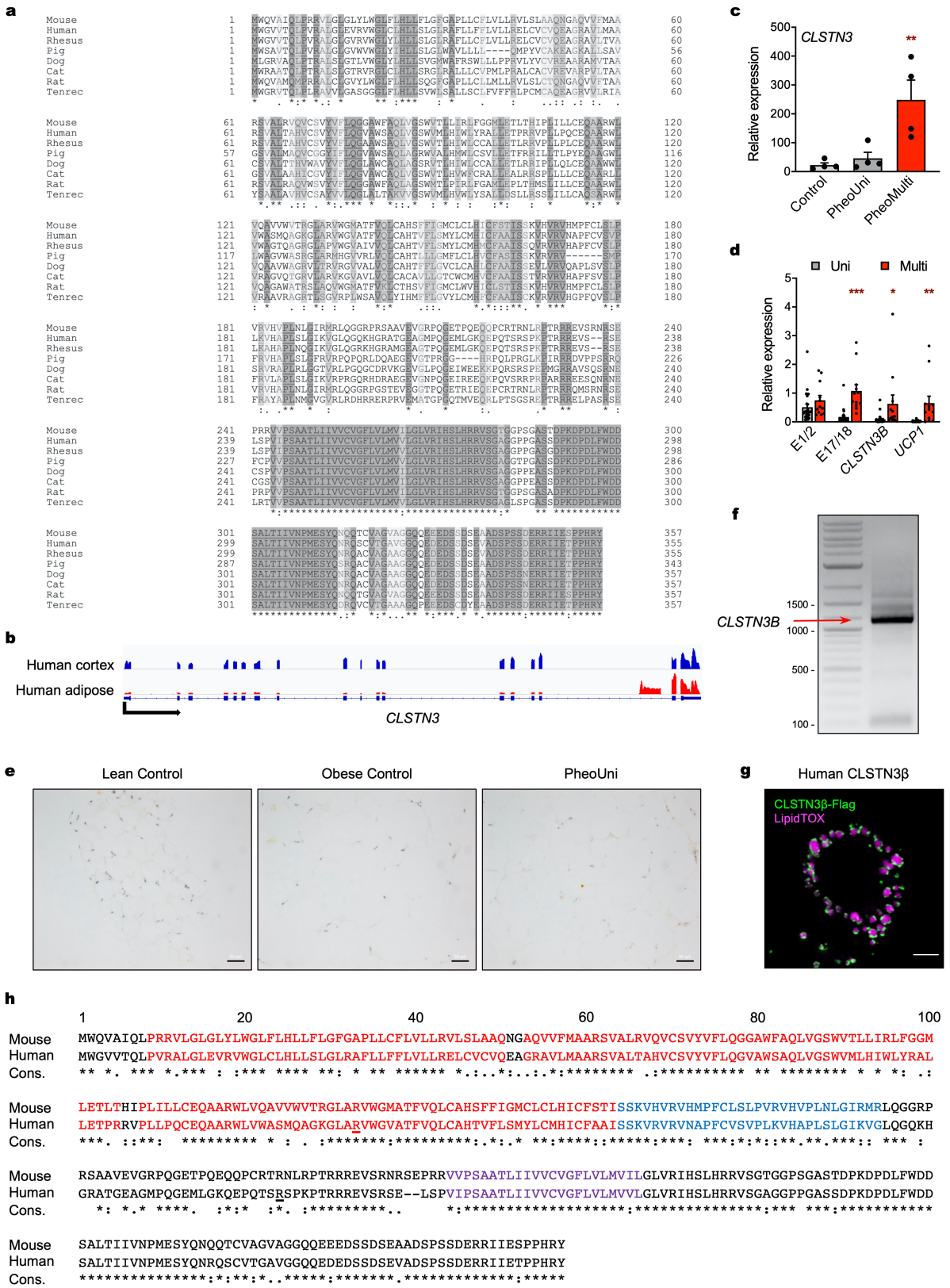

Extended Data Fig. 10 | See next page for caption.

Extended Data Fig. 10 | Conservation of *CLSTN3B* in humans. a, Amino acid alignment of CLSTN3β from representative placental mammals. **b**, RNA-seq reads at the *CLSTN3* locus in human cortex and adipose tissue. **c**, Microarray analysis of *CLSTN3* expression in periadrenal adipose tissue from control patients, pheochromocytoma patients with unilocular fat (PheoUni), and pheochromocytoma patients with multilocular fat (PheoMulti) ($n = 4$). **d**, qPCR analysis of *CLSTN3* exons 1/2, *CLSTN3* exons 17/18, *CLSTN3B*, and *UCP1* expression in human unilocular and multilocular adipose tissue ($n = 26, 12$). Unilocular group includes both control and PheoUni patients. **e**, RNAscope analysis of *CLSTN3B* expression in unilocular periadrenal adipose tissue from lean control, obese control, and pheochromocytoma (PheoUni) patients. Scale bar = 50 µm. **f**, Cloning of human *CLSTN3B*. **g**, Confocal microscopy of OA-treated (1 mM, overnight) HeLa cells transfected with human CLSTN3β-Flag and stained with LipidTOX 647. Scale bar = 5 µm. **h**, Amino acid alignment of mouse and human CLSTN3β (reference sequences). Putative hydrophobic hairpins, β-strand domain, and TM domain are colored red, blue, and purple, respectively. Underlined residues are altered in the patient from which human CLSTN3β was cloned for this study. Bar plots show mean ± SEM. Each point represents a biological replicate. Two-sided $^{*}P < 0.05$, $^{**}P < 0.01$, $^{***}P < 0.001$ by ordinary one-way ANOVA with Dunnett's multiple comparisons test (**c**) or multiple t-tests with Holm-Sidak correction (**d**).

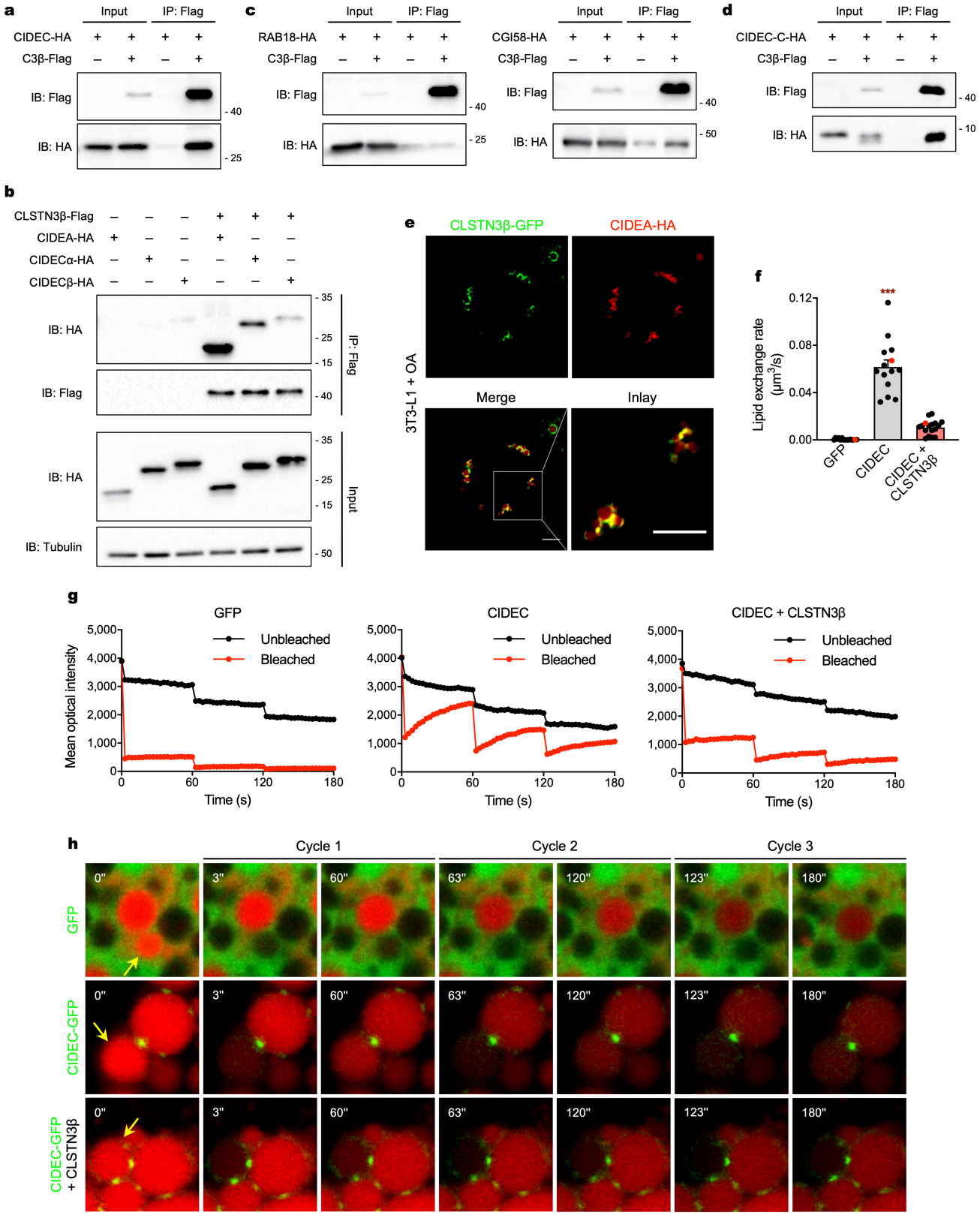

Extended Data Fig. 11 | CLSTN3β associates with CIDE proteins and blocks LD fusion. (**a**–**d**) Western blot analysis of CLSTN3β-Flag co-immunoprecipitation assays in transfected HEK293FT cells. **a**, CIDEC-HA, **b**, CIDEA-HA, CIDECα-HA, and CIDECβ-HA, **c**, RAB18-HA and CGI58-HA, **d**, HA-tagged CIDEC C-terminal region (CIDEC-C-HA). **e**, Co-localization of CLSTN3β-GFP and CIDEA-HA in transfected 3T3-L1 preadipocytes treated with OA. Scale bar = 5 μm. (**f**–**h**) Fluorescence recovery after photobleaching (FRAP)-based lipid exchange rate assay in transfected 3T3-L1 preadipocytes incubated with 200 μM OA and 1 μg/mL BODIPY 558/568 C_{12} fatty acid for 16 h. **f**, Calculated lipid exchange rates (n = 15, 14, 17 cells). Cells used for representative traces are highlighted in red. **g**, Representative mean optical intensity traces for one pair of LDs from each group. **h**, Representative images of FRAP-based lipid exchange rate assay. Yellow arrows point to bleached LDs. Bar plots show mean ± SEM. Each point represents a biological replicate. Two-sided ***P < 0.001 by ordinary one-way ANOVA with Tukey's multiple comparisons test (**f**).

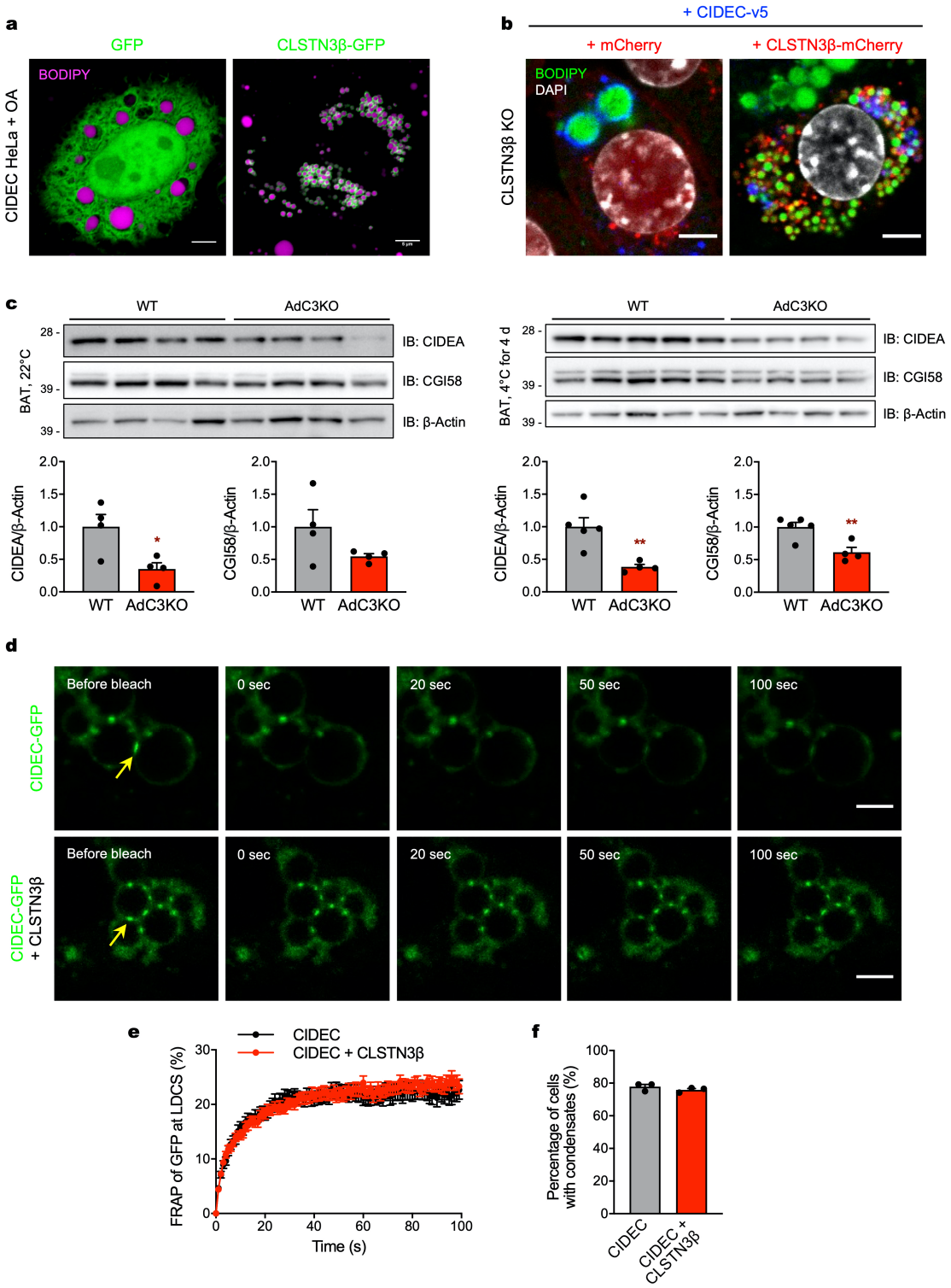

Extended Data Fig. 12 | CLSTN3β associates with CIDE proteins and blocks LD fusion. a, Confocal microscopy of HeLa cells stably expressing CIDEC and transiently expressing either GFP or CLSTN3β-GFP. Cells were treated with OA and LDs were stained with BODIPY 665. Scale bar = 5 µm. **b**, Confocal microscopy of immortalized CLSTN3β KO brown adipocytes stably expressing mCherry or CLSTN3β-mCherry and CIDEC-v5 (day 5 of differentiation). Cells were stained with BODIPY 488, DAPI, and anti-v5, and mCherry signal was amplified with anti-mCherry Alexa Fluor 594. Scale bar = 5 µm. **c**, (Top) Western blot analysis of BAT from male WT and AdC3KO mice housed at (left) 22 °C or (right) 4 °C for 4 days. (Bottom) Quantification of above Western blots. **d**, Representative images of FRAP-based phase separation assay. Yellow arrows point to bleached signal at LD–LD contact sites (LDCS). Scale bar = 2 µm. **e**, Quantification of FRAP-based phase separation assay ($n = 22$ cells). **f**, Percentage of cells with CIDEC condensates in the absence or presence of CLSTN3β ($n = 3$). Bar/line plots show mean ± SEM. Each point represents a biological replicate. Two-sided $^{*}P < 0.05$, $^{**}P < 0.01$ by Welch's t-test (**c**).

nature portfolio

Corresponding author(s): Peter Tontonoz

Last updated by author(s): Oct 5, 2022

Reporting Summary

Nature Portfolio wishes to improve the reproducibility of the work that we publish. This form provides structure for consistency and transparency in reporting. For further information on Nature Portfolio policies, see our Editorial Policies and the Editorial Policy Checklist.

Statistics

For all statistical analyses, confirm that the following items are present in the figure legend, table legend, main text, or Methods section.

n/a	Confirmed
☐	☒ The exact sample size (*n*) for each experimental group/condition, given as a discrete number and unit of measurement
☐	☒ A statement on whether measurements were taken from distinct samples or whether the same sample was measured repeatedly
☐	☒ The statistical test(s) used AND whether they are one- or two-sided *Only common tests should be described solely by name; describe more complex techniques in the Methods section.*
☒	☐ A description of all covariates tested
☐	☒ A description of any assumptions or corrections, such as tests of normality and adjustment for multiple comparisons
☐	☒ A full description of the statistical parameters including central tendency (e.g. means) or other basic estimates (e.g. regression coefficient) AND variation (e.g. standard deviation) or associated estimates of uncertainty (e.g. confidence intervals)
☐	☒ For null hypothesis testing, the test statistic (e.g. *F*, *t*, *r*) with confidence intervals, effect sizes, degrees of freedom and *P* value noted *Give P values as exact values whenever suitable.*
☒	☐ For Bayesian analysis, information on the choice of priors and Markov chain Monte Carlo settings
☒	☐ For hierarchical and complex designs, identification of the appropriate level for tests and full reporting of outcomes
☒	☐ Estimates of effect sizes (e.g. Cohen's *d*, Pearson's *r*), indicating how they were calculated

Our web collection on statistics for biologists contains articles on many of the points above.

Software and code

Policy information about availability of computer code

Data collection	Leica Application Suite X, Zeiss ZEN 2 Pro, ImSpector Pro v7.1.0, EchoMRI v120711, Oxymax/CLAMS v5.25.05, Syngene PXi v1.8.5.0, ImageQuant LAS 4000 v1.2, CLARIOstar v5.20 R5, QuantStudio v1.1, Seahorse XF24
Data analysis	Microsoft Excel for Mac v16.65, GraphPad Prism 8, ImageJ v2.1.0/1.53c, RStudio v1.3.1093, MATLAB R2016a, CellProfiler v4.2.1, FastQC v0.11.8, Trimmomatic v0.39, STAR, HTSeq, DESeq2 v1.30.0, LeafCutter, Mascot Daemon v2.3, MaxQuant v1.6.3.3

For manuscripts utilizing custom algorithms or software that are central to the research but not yet described in published literature, software must be made available to editors and reviewers. We strongly encourage code deposition in a community repository (e.g. GitHub). See the Nature Portfolio guidelines for submitting code & software for further information.

Data

Policy information about availability of data

All manuscripts must include a data availability statement. This statement should provide the following information, where applicable:

- Accession codes, unique identifiers, or web links for publicly available datasets
- A description of any restrictions on data availability
- For clinical datasets or third party data, please ensure that the statement adheres to our policy

Source data for all figures are provided with the paper. The RNA sequencing dataset generated for this paper is available at accession number GSE181123. The previously published RNA sequencing dataset used for LeafCutter splicing analysis in this paper is available at accession number GSE65776.

Field-specific reporting

Please select the one below that is the best fit for your research. If you are not sure, read the appropriate sections before making your selection.

☒ Life sciences ☐ Behavioural & social sciences ☐ Ecological, evolutionary & environmental sciences

For a reference copy of the document with all sections, see nature.com/documents/nr-reporting-summary-flat.pdf

Life sciences study design

All studies must disclose on these points even when the disclosure is negative.

Sample size	No explicit sample-size calculations were performed. Sample sizes were determined based on our past experience in the field and informed by similar experiments described in the published literature, particularly those with effect sizes that were expected to be comparable to our own.
Data exclusions	No data were excluded from the analyses.
Replication	All findings were reproduced at least twice by replicating the experiments and/or cross-validating with orthogonal approaches.
Randomization	Allocation was generally not randomized because experimental groups were generally separated by genotype. If a single genotype was sub-divided into multiple experimental groups, then allocation was randomized.
Blinding	Investigators were generally not blinded to group allocation during data collection and analysis. For cell-based experiments, group allocation and data collection/analysis were performed by the same investigators, so blinding could not reasonably be achieved. For mouse-based experiments, mice were genotyped prior to group allocation to ensure that group sizes would be sufficient, thereby unblinding the investigators. Blinding during data analysis was ensured for one experiment: quantification of sympathetic innervation in cleared BAT (Extended Data Fig. 8B-D). In this case, a specific investigator not otherwise involved in the experiment was provided with unlabeled image files for analysis.

Reporting for specific materials, systems and methods

We require information from authors about some types of materials, experimental systems and methods used in many studies. Here, indicate whether each material, system or method listed is relevant to your study. If you are not sure if a list item applies to your research, read the appropriate section before selecting a response.

Materials & experimental systems

n/a	Involved in the study
☐	☒ Antibodies
☐	☒ Eukaryotic cell lines
☒	☐ Palaeontology and archaeology
☐	☒ Animals and other organisms
☐	☒ Human research participants
☒	☐ Clinical data
☒	☐ Dual use research of concern

Methods

n/a	Involved in the study
☒	☐ ChIP-seq
☒	☐ Flow cytometry
☒	☐ MRI-based neuroimaging

Antibodies

Antibodies used

ATGL (30A4) Cell Signaling #2439 - WB 1:1000
Calnexin Abcam ab10286 - WB 1:1000
Calreticulin (D3E6) Cell Signaling #12238 - WB 1:1000
CGI58 (EPR12621) Abcam ab183739 - WB 1:1000
CIDEA Proteintech 13170-1-AP - WB 1:1000
CLSTN3 Proteintech 13302-1-AP - WB 1:1000, IP 1:100, IHC 1:100
FABP4 (B-4) Santa Cruz sc-271529 - WB 1:5000
Flag (M2) MilliporeSigma F1804 - WB 1:2000, IF 1:500
gp78/AMFR Cell Signaling #9590 - WB 1:1000
GRP94 (9G10) ThermoFisher MA3-016 - WB 1:1000
HA (C29F4) Cell Signaling #3724 - WB 1:1000, IF 1:500
HSL Cell Signaling #4107 - WB 1:2000
mCherry AF594 (16D7) ThermoFisher M11240 - IF 1:1000
Myc (4A6) MilliporeSigma 05-724 - WB 1:1000
Normal Rabbit IgG Cell Signaling #2729 - ChIP 1:100
OXPHOS Abcam ab110413 - WB 1:5000
p-HSL S563 Cell Signaling #4139 - WB 1:1000
p-HSL S660 Cell Signaling #4126 - WB 1:1000

PLIN1 (D1D8) Cell Signaling #9349 - WB 1:1000
PLIN2 (EPR3713) Abcam ab108323 - WB 1:1000
PPARg (81B8) Cell Signaling #2443 - ChIP 1:100
p-PKA substrate (100G7E) Cell Signaling #9624 - WB 1:1000
S100B (EP1576Y) Abcam ab52642 - WB 1:1000
S6 (54D2) Cell Signaling #2317 - WB 1:1000
TH (mouse, LNC1) MilliporeSigma MAB318 - WB 1:1000
TH (sheep) MilliporeSigma AB1542 - AdipoClear 1:200
TIMM23 Proteintech 11123-1-AP - WB 1:1000
TOMM20 Proteintech 11802-1-AP - WB 1:1000
Ubiquitin Proteintech 10201-2-AP - WB 1:1000
UCP1 Abcam ab10983 - WB 1:5000
V5 Cell Signaling #13202 - IF 1:500
Beta-Actin MilliporeSigma A2066 - WB 1:2000
Beta-Tubulin Abcam ab15568 - WB 1:2000
Donkey anti-sheep IgG AF568 - AdipoClear 1:200

Validation

CLSTN3 antibody was knockout-validated in this study for Western blot, immunoprecipitation, and immunohistochemistry analysis of mouse cells and tissues (Extended Data Fig. 2A, 2E, 5B, 9G).

ATGL - https://www.cellsignal.com/products/primary-antibodies/atgl-30a4-rabbit-mab/2439
Calnexin - https://www.abcam.com/calnexin-antibody-ab10286.html
Calreticulin - https://www.cellsignal.com/products/primary-antibodies/calreticulin-d3e6-xp-rabbit-mab/12238
CGI58 - https://www.abcam.com/nav/primary-antibodies/rabbit-monoclonal-antibodies/abhd5cgi-58-antibody-epr12621-ab183739.html
CIDEA - https://www.ptglab.com/products/CIDEA-Antibody-13170-1-AP.htm
FABP4 - https://www.scbt.com/p/a-fabp-antibody-b-4
Flag - https://www.sigmaaldrich.com/US/en/product/sigma/f1804
gp78/AMFR - https://www.cellsignal.com/products/primary-antibodies/amfr-antibody/9590
GRP94 - https://www.thermofisher.com/antibody/product/GRP94-Antibody-clone-9G10-Monoclonal/MA3-016
HA - https://www.cellsignal.com/products/primary-antibodies/ha-tag-c29f4-rabbit-mab/3724
HSL - https://www.cellsignal.com/products/primary-antibodies/hsl-antibody/4107
mCherry AF594 - https://www.thermofisher.com/antibody/product/mCherry-Antibody-clone-16D7-Monoclonal/M11240
Myc - https://www.emdmillipore.com/US/en/product/Anti-Myc-Tag-Antibody-clone-4A6,MM_NF-05-724
Normal Rabbit IgG - https://www.cellsignal.com/products/primary-antibodies/normal-rabbit-igg/2729
OXPHOS - https://www.abcam.com/total-oxphos-rodent-wb-antibody-cocktail-ab110413.html
p-HSL S563 - https://www.cellsignal.com/products/primary-antibodies/phospho-hsl-ser563-antibody/4139
p-HSL S660 - https://www.cellsignal.com/products/primary-antibodies/phospho-hsl-ser660-antibody/4126
PLIN1 - https://www.cellsignal.com/products/primary-antibodies/perilipin-1-d1d8-xp-rabbit-mab/9349
PLIN2 - https://www.abcam.com/adfp-antibody-epr3713-ab108323.html
PPARg - https://www.cellsignal.com/products/primary-antibodies/pparg-81b8-rabbit-mab/2443
p-PKA substrate - https://www.cellsignal.com/products/primary-antibodies/phospho-pka-substrate-rrxs-t-100g7e-rabbit-mab/9624
S100B - https://www.abcam.com/s100-beta-antibody-ep1576y-astrocyte-marker-ab52642.html
S6 - https://www.cellsignal.com/products/primary-antibodies/s6-ribosomal-protein-54d2-mouse-mab/2317
TH (mouse) - https://www.emdmillipore.com/US/en/product/Anti-Tyrosine-Hydroxylase-Antibody-clone-LNC1,MM_NF-MAB318
TH (sheep) - https://www.emdmillipore.com/US/en/product/Anti-Tyrosine-Hydroxylase-Antibody,MM_NF-AB1542
TIMM23 - https://www.ptglab.com/products/TIMM23-Antibody-11123-1-AP.htm
TOMM20 - https://www.ptglab.com/products/TOM20-Antibody-11802-1-AP.htm
Ubiquitin - https://www.ptglab.com/products/ubiquitin-Antibody-10201-2-AP.htm
UCP1 - https://www.abcam.com/ucp1-antibody-ab10983.html
V5 - https://www.cellsignal.com/products/primary-antibodies/v5-tag-d3h8q-rabbit-mab/13202
Beta-Actin - https://www.sigmaaldrich.com/US/en/product/sigma/a2066
Beta-Tubulin - https://www.abcam.com/beta-tubulin-antibody-ab15568.html
Donkey anti-sheep IgG AF568 - https://www.thermofisher.com/antibody/product/Donkey-anti-Sheep-IgG-H-L-Cross-Adsorbed-Secondary-Antibody-Polyclonal/A-21099

Eukaryotic cell lines

Policy information about cell lines

Cell line source(s)	HEK293T (ATCC), HeLa (ATCC), 3T3-L1 (ATCC), C3H/10T1/2 (ATCC), 3T3-F442A (ECACC), immortalized brown preadipocytes (Tontonoz)
Authentication	Commercial cell lines were authenticated by commercial vendors (STR profiling). Tontonoz lab cell line was authenticated by morphology and our previously published NGS data (PMID 29249357).
Mycoplasma contamination	The cell lines were not routinely tested for mycoplasma contamination.
Commonly misidentified lines (See ICLAC register)	No commonly misidentified cell lines were used in the study.

Animals and other organisms

Policy information about studies involving animals; ARRIVE guidelines recommended for reporting animal research

Laboratory animals	Mus musculus, C57BL/6N and J (ob/ob), male and female, 1-6 months old
Wild animals	The study did not involve wild animals.
Field-collected samples	The study did not involve samples collected from the field.
Ethics oversight	Mouse studies were approved by the Chancellor's Animal Research Committee.

Note that full information on the approval of the study protocol must also be provided in the manuscript.

Human research participants

Policy information about studies involving human research participants

Population characteristics	All information about human research participants was published in a previous study, which has been referenced in this manuscript. No human research participants were recruited specifically for this study. In brief, the patient cohort was approximately 50% male and 50% female with an average patient age of approximately 50. Patients in the experimental group had sporadic unilateral benign adrenal pheochromocytomas, while patients in the control group had aldosterone-secreting, cortisol-secreting, or non-functioning neoplasms.
Recruitment	All information about human research participants was published in a previous study, which has been referenced in this manuscript. No human research participants were recruited specifically for this study. In brief, each patient provided written consent after the study goals, side effects, and tissue sampling procedure were explained in detail.
Ethics oversight	All information about human research participants was published in a previous study, which has been referenced in this manuscript. No human research participants were recruited specifically for this study. In brief, the study protocol was reviewed and approved by the UCLA Medical Institutional Review Board.

Note that full information on the approval of the study protocol must also be provided in the manuscript.